Chapter 10.

NON-LINEAR DYNAMICS OF AU IN HYDROTHERMAL SYSTEMS OF THE ARCHAEAN YILGARN CRATON, WESTERN AUSTRALIA.

May_23_2016.

10.1. Introduction.

Since nonlinear dynamical systems, including hydrothermal systems, can evolve as chaotic systems a very large number of states can be occupied by the system both in space and time. Just as in classical statistical mechanics as developed by Gibbs in 1902 one can define average quantities such as pressure, temperature and entropy for a system of molecules, these same quantities (but with different physical meanings) can be defined for chaotic systems; this leads to the thermodynamics of chaotic systems as developed by many but exemplified in the book by Beck and Schlögl in 1993. In chaotic systems the entropy function is commonly called the multifractal singularity spectrum.

The singularity spectrum characterises the range of fractal dimensions developed in the system and the singularities (places corresponding to high or low concentrations of these fractal dimensions) corresponding to these fractal dimensions. Thus one hallmark of a chaotic system is its singularity spectrum; the other hallmark is the attractor that describes the dynamics of the system. In this chapter we explore the singularity spectra of gold concentration for seven gold ore bodies in the Yilgarn of Western Australia. We report on 875 different spectra.

In principle the singularity spectrum, together with its associated wavelet transform scalogram of the initial data, contain all the information we need to understand the multiplicative processes involved in the formation of the system. The mere existence of a singularity spectrum indicates the system is multifractal (rather than monofractal, periodic or random corresponding to white noise) and hence is the result of some deterministic process. The metrics of the spectra (width, asymmetry values of the fractal dimension for a given tangent slope) give information on the dynamics and provide quantitative measures that enable one to describe, compare and contrast different chaotic systems.

The goal we seek is some discriminator between well-endowed and poorly endowed gold systems. We present progress in attaining this goal in this chapter.

10.2. Ore bodies studied within the Archaean Yilgarn Craton.

Wavelet-based analysis is applied to a number of ore bodies hosted in the Archaean Greenstone belt of the Eastern Goldfields Superterrane, Archaean Yilgarn Craton, Western Australia to evaluate the non-linear dynamics of these systems. These include a range of spatially and structurally distinct ore bodies from the Sunrise Dam deposit, and the Majestic/Imperial and Salt Creek prospects from the Yindarlgooda dome region of the Mount Monger goldfield (Figure 10.1). These deposits were selected because they present a range of structural and alteration histories, as well as a range of Au grades and endowments.

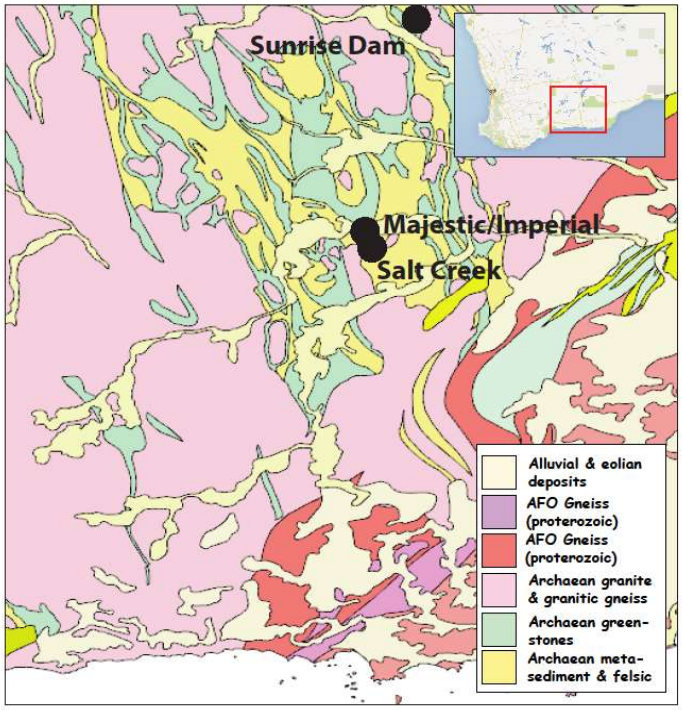

Figure 10.1. Interpreted regional-scale bedrock and surficial geology map of the Archaean Yilgarn craton of Western Australia showing the locations of ore bodies analysed from the Archaean greenstone belt. Inset marks the geographical position of the geology map in the southwest of the Australian continent. Bedrock geology map modified from the Geological Survey of Western Australia (GSWA) online interactive map.

10.2.1 The Sunrise Dam system.

The Late Archaean Sunrise Dam deposit is situated in the Laverton tectonic zone of the Kurnalpi terrane. Dated ~2670Ma, the deposit is hosted by volcaniclastics (basaltic to andesitic) and banded iron formation (magnetite-rich shales and turbidites). These country rocks have been intruded by a series of sills and dykes - primarily quartz-feldspar porphyry, but locally lamprophyres and ultramafics. Peak metamorphic conditions are greenschist facies, however the timing of Au and sulphide mineralization relative to this remains unconstrained. The broader-scale Sunrise Dam system is sub-divided into several structurally and petrologically distinct ore bodies of differing size and grade (Figure 10.2).

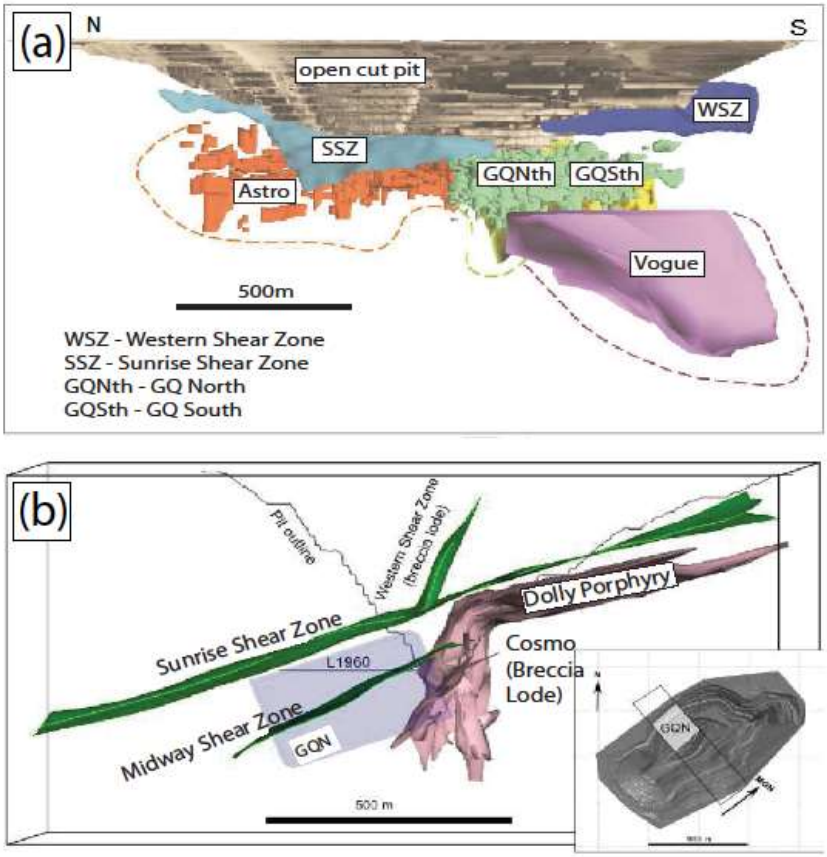

Figure 10.2. (a) North-south (mine-grid) cross-section of 3D model of the ore bodies at Sunrise Dam, showing their relationship to the mine pit. Drill core from Vogue, GQ (North & South) and Astro are used in this study. (b) Cross-section view of a 3D model showing the Cosmo breccia lode and its relationship to the Dolly porphyry, prominent shear zones and GQ North. (a) and (b) modified from Hill et al., 2014.

A convoluted seven-stage structural evolution has been recognised at Sunrise Dam. Throughout this deformation chronology, weak Au mineralization (~0.25-1.5g/t) accompanied D_1, with stronger mineralization associated with D_3, D_{4a} and D_{4b} (averaging grades of 2.8g/t, 16.5g/t and 4.25-18g/t, respectively). Using this deformation chronology and mineralization history, investigations of the deposit have proposed a four-group classification scheme for the Au lodes (I, II, III & IV) based principally upon their dominant hosting structures. This study presents wavelet-based analysis of lodes from within each of the groups: Vogue, GQ, Cosmo East and Astro.

Group I ore bodies are hosted primarily within gently to moderately (~20-40°) northwest-dipping shear zones associated with northwest-directed thrusting (the GQ, Mako, Sunrise, Midway and Cleo). Au mineralization is hosted within quartz-carbonate ± pyrite ± arsenopyrite veins within an intense penetrative chlorite-sericite D_3 fabric. Associated wall-rock alteration consists of the assemblage quartz-sericite-carbonate-pyrite-chlorite. Mineralization in Group I is also hosted in younger laminated quartz-carbonate veins that cross-cut syn-D_3 veining (interpreted as syn-D_4).

Group II ore bodies are dominantly breccia- and vein-hosted, situated within steeply-dipping D_3 shear zones such as the Summercloud, Watu and Predator. Mineralization is also (less frequently) contained within penetrative fabrics. Localized zones of brecciation may be up to several metres wide, consisting of angular sericite-replaced volcanic clasts encased within quartz-carbonate cements. Veining (often steeply dipping) may be up to 5m in width, composed of

carbonate-pyrite-arsenopyrite-quartz. Other gently northwest-dipping veins containing Au, tellurides and As sulphides have been interpreted as syn-D_4, contemporaneous with dextral normal faulting.

Group III type ore bodies (e.g. the Cosmo and Dolly lodes) are hosted within zones of stockwork veins and brecciation up to 20m across. Stockwork veining contains carbonate-chlorite-quartz ± sericite ± pyrite ± arsenopyrite, associated with sericite-quartz-pyrite-ankerite ± arsenopyrite alteration of the surrounding volcanic host rocks. Breccia clasts are cemented by quartz and carbonate. Group III ore bodies are primarily associated with D_{4a} deformation, characterized by northeast bulk shortening and dextral fault kinematics.

Group IV ore bodies encompass those hosted within the extensively sericite-altered Dolly quartz-feldspar porphyry, where mineralization is contained within narrow steep, As-rich veining. Within this four-group classification system, the GQ and Astro ore bodies analysed in this study constitute part of Group I - those hosted in gently to moderately northwesterly-dipping shear zones. Cosmo East forms part of the Group III stockwork vein and breccia lodes.

10.2.2 The Yindarlgooda Dome – Majestic/Imperial and Salt Creek.

10.2.2.1. Regional tectono-metamorphic evolution.

The Yindarlgooda Dome (Figure 10.3) is situated ~50km due east of Kalgoorlie in the Gindalbie domain of the Kurnalpi terrane. The core of the dome is composed of granite, which has intruded through a sequence of felsic to intermediate volcanics and volcaniclastics. The region of the Kurnalpi terrain has experienced a four-stage deformation history. Approximately north-south directed bulk shortening during D_1 produced east-west trending isoclinal and recumbent folds, and thrusts. D_2 east-northeast – west-southwest bulk shortening produced upright north-northwest – south-southeast trending folds with a steeply dipping axial plane foliation. Transpression during D_3 resulted in left-lateral motion along ductile shear zones and brittle faults. D_4 bulk shortening produced a series of conjugate oblique-slip faults, with a sinistral component of strike-slip motion along those that are north-northwest to northwest striking and dextral/reverse motion on those that are northeast to east-northeast striking. This was also associated with a locally developed crenulation cleavage and kink-style folding. Regional peak metamorphic grade is generally greenschist facies, locally enhanced to amphibolite facies adjacent to emplaced granitoids (many of which post-date regional-scale folding).

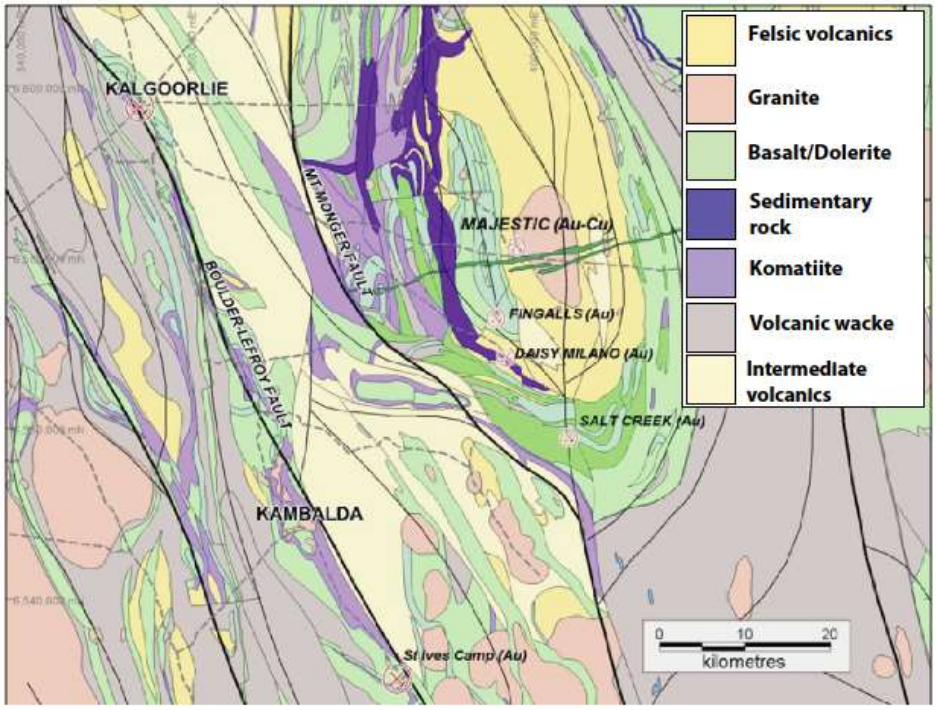

Figure 10.3. Regional-scale interpreted bedrock geology of the Yindarlgooda Dome, indicating the positions of Majestic/Imperial and Salt Creek. Salt Creek is situated on the western limb of the Southward-plunging Bulong Anticline at the Southern end of the Yindarlgooda Dome. Majestic and Imperial are situated on the western limb of the Bulong Anticline, on the western side of the Juglah Monzogranite. After Young, 2012.

10.2.2.2. Majestic & Imperial.

The Majestic project is situated on the western limb of the Bulong Anticline (Figure 10.3) on the western side of the Juglah Monzogranite. The monzogranite was emplaced within a sequence of intermediate to felsic volcanic and volcaniclastic rocks, the contact of which is poorly exposed due to the overlying regolith. The Majestic project is sub-divided into two economic deposits (Majestic and Imperial) both of which are situated structurally below westward-dipping 'D1' thrusts. The Majestic and Imperial ore bodies are genetically related - separated by left-lateral strike-slip motion along a major northwest-southeast striking fault at the northern margin of Majestic (Figure 10.4).

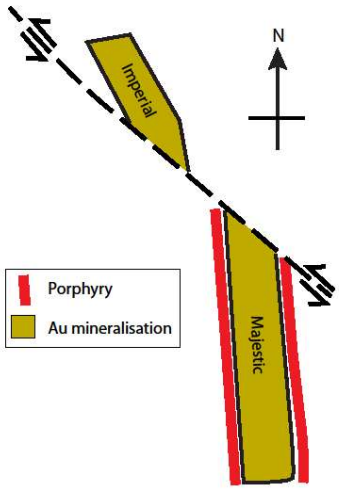

Figure 10.4. Schematic plan-view sketch of the spatial relationship of the Majestic and Imperial ore bodies. Sinistral relative motion on the northwest-southeast striking shear zone has offset Imperial from the rest of the Majestic ore body.

Imperial is less spatially extensive than Majestic, but has higher mean Au grades.

The Majestic project is primarily hosted within a weakly porphyritic quartz-diorite stock, itself intruded by a swarm of tonalite dykes. Two styles of Au mineralization have been identified: I) a texturally earlier stage spatially associated with biotite-pyrite alteration, and II) a texturally younger stage spatially associated with an albite-silica-pyrite 'bleaching' with minor sericite, pyrrhotite and chalcopyrite. The earlier (biotite-pyrite associated) phase of Au mineralization is structurally controlled; with greater alteration intensity and Au grades preferentially developed within, and surrounding, breccia and fracture networks. Biotite-pyrite alteration is manifest at scales up to tens of metres, spatially associated with a series of tonalite porphyry dykes (considered as the driving mechanism for biotite-associated Au mineralization).

The second (albite-silica-pyrite) stage of alteration is spatially more localised than the first - manifest from the mm-scale to zones several metres across. Structurally, this sodic style of alteration is localised along breccias, veining, brittle-ductile shears and fractures that predominantly post-date zones of biotite-pyrite alteration. However, mutual overprinting between the two alteration styles is locally observed, suggesting that they were broadly contemporaneous. Where both stages of alteration overprint one another, strongly elevated Au grades are observed.

The two mineralization-related alteration stages at Majestic are post-dated by three vein-forming stages; the first associated with laminated quartz and quartz-carbonate veins, the second epidote-calcite veins (with locally developed epidote-hematite-albite wall-rock alteration) and the third carbonate-gypsum veins. A strong ~1-10m wide supergene enrichment zone is developed at depths of ~30-60m above the hypogene sections of the Majestic system. This has produced a characteristic depletion in Au and Cu grades in the weathered zone of 'lower saprolite' above, remobilizing it for re-precipitation at concentrations typically between 0.5-2g/t along the enrichment zone. This supergene remobilization of Au has produced a large 'footprint' 100's of metres wide - significantly larger than the primary hypogene zone itself (~20m wide).

10.2.2.3. Salt Creek.

The Salt Creek prospect is situated at the southern end of the Yindarlgooda Dome, on the western limb of the southward-plunging Bulong Anticline (Figure 10.3). Mineralization is primarily hosted within quartz-magnetite dolerite, which constitutes one unit of the differentiated doleritic to gabbroic 'Salt Creek sill'. The sill is one of a number that intrude into a series of dominantly high-Mg basaltic volcanics (the Bulong complex) and are folded about the Bulong anticline (interpreted as a regional D_2 structure). The sill dips ~60° to the southwest, with a true thickness of ~250m.

The Salt Creek Sill is subdivided into lithologies (Figure 10.5); the contacts between which are gradational, interpreted to reflect the fractionation of mafic magma. Units I and V (the top and base of the sill, respectively) are composed of fine-grained dolerite with a massive texture, interpreted as chilled margins. Unit II is a fine-grained, ~20-30m thick, zone characterized by the presence of large (2-5mm) primary titanomagnetite crystals that compose ~2-5% of the rock volume. Unit III is a quartz-magnetite dolerite that ranges up to 150m in thickness, defined primarily by elevated quartz (typically 20-30%) in the form of 'blue quartz eyes'. In proximity to its base, Unit III grades into a 'bladed' leucodolerite, before transitioning into the coarser-grained leucogabbro that defines Unit IV. The Unit IV leucogabbro is equigranular and possesses a greater felsic component than mafic.

Au mineralization at Salt Creek is largely contained within the quartz-magnetite dolerite and leucodolerite of Unit III (Figure 10.5), with the width of the mineralized zone ranging from 2-80m. Two primary mineralization styles have been distinguished, with Au being almost entirely vein-hosted. The first is a steeply (~65°) eastward-dipping zone of intense quartz-carbonate veining, shear zones and brecciation - labeled the Salt Creek Fault Zone. This 'structural core' is associated with intense silica, albite and pyrrhotite wall-rock alteration and extensional-shear type veins.

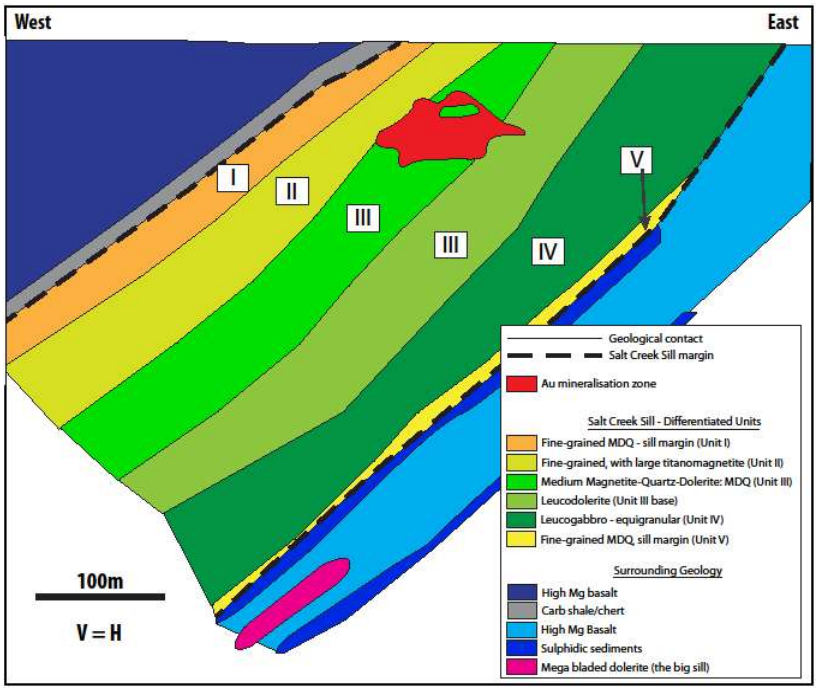

Figure 10.5. East-west oriented structural cross-section of the Salt Creek Sill, displaying the five differentiated units and the position of mineralization (confined to within Unit III). True scale (V = H). Modified from 2008 Integra report.

The second style consists of a shallow to moderately westward-dipping vein array that surrounds the steeply eastward-dipping 'structural core' mineralization. This strong alteration selvage is associated with albite, sericite, silica and pyrrhotite (± pyrite). Structurally, the second alteration style appears partitioned along the steep westward dip of the sills and stratigraphic sequences, in the hanging wall of the Salt Creek Fault Zone.

Within this framework, 10 vein types were identified; four of which are associated with the ore zone within Unit III. Three of these four vein types associated with mineralization are pyrrhotite-bearing, to which Au shows a strong spatial correlation. Veins associated with mineralization are dominantly extensional and extensional-shear (hybrid) type. In the mineralized zones, sulphides (pyrrhotite and pyrite) typically compose 1-5% of the rock volume. During the structural evolution, an array of brittle-ductile chlorite and biotite- shears interpreted to cross-cut the Salt Creek Sill served as important conduits for the flux and localization of Au and Cu-bearing fluids.

Au grades in the two mineralization zones are locally elevated above a general minimum threshold of 0.5g/t. Visible Au at Salt Creek is rare. Moreover, Au is extremely fine-grained (potentially sub-microscopic) being rarely observed under standard optical and Scanning Electron (SEM) microscopy. In addition to the strong proximate albite-sericite-silica-pyrrhotite alteration zones associated with the two styles of Au mineralization, a broader-scale chlorite alteration zone surrounds Salt Creek.

10.3. Drill core orientations and Au assay data acquisition.

Drilling programs in the Imperial, Majestic and Salt Creek prospects of the Yindarlgooda Dome use reverse circulation (RC) drilling from the surface. Significant Au and element mobilization may occur within the regolith profile modifying their initial spatial organization. The unconsolidated regolith portion at the top of each drill-core (up to ~60m deep) was removed prior to wavelet analysis so that only fresh bedrock intervals were analysed. Drill cores analysed at Salt Creek form a sub-parallel steeply northeasterly dipping array, spaced 10m apart. Those analysed from Imperial and Majestic are also in sub-parallel arrays that dip steeply due east.

Drilling at Sunrise Dam involves two types of diamond drill hole; those initiated from the surface (designated CD) and those initiated from underground drives (designated UGD). Typically, the upper ~50-100m of CD holes is composed of unconsolidated regolith in palaeochannels, whereas the entire span of UGD holes intersect consolidated bedrock. Therefore, the regolith profiles in CD holes were removed prior to wavelet application and only fresh bedrock analysed. Hole intervals analysed at Sunrise Dam range from 39-508m, averaging 188±83m. Sunrise Dam drill cores are more variably oriented through the ore bodies than those in the Yindarlgooda dome.

Drill cores in all ore bodies examined from the Yindarlgooda Dome and Sunrise Dam were sectioned into consistent 100m intervals with 1m resolution Au assays. Au assay concentrations data for all deposits were converted into the same format (0.01ppm resolution). Where the remaining portion at the end of the hole was equal to or greater than 25m, an additional interval was analysed that partially overlaps with the interval above. This was conducted to utilise the maximum amount of drill core material possible.

10.4. Wavelet analysis: Procedure.

The Wavelet Transform Modulus Maxima (WTMM) method was applied to the down-hole Au assay data using LastWave 3.1 for Windows. The well-established 'Mexican Hat' wavelet (2^{nd} derivative of the Gaussian distribution) was selected due to its geometry being applicable to the peaks and troughs in concentration commonly observed in Au assay and hyperspectral mineral abundance datasets. The scale-adapted method of WTMM was used, which employs varying sizes of the mother wavelet. The maximum permitted wavelet size was applied to furnish the highest resolution of wavelet transform scalogram (one octave sub-divided into 20 voices). Consistent wavelet parameters were applied to the datasets from both Sunrise Dam and the Yindarlgooda Dome. In conjunction with a consistent Au assay dataset size and resolution in ppm, this ensures that differences between singularity spectra reflect fundamental geological processes and not variations in dataset format. Examples of some of the wavelet transforms and singularity spectra are given in Chapter xx and in Ord, Munro and Hobbs (2016).

10.5. Au spatial organisation in ore bodies of the Archaean Yilgarn Craton.

The following section compares the key features of 875 singularity spectra derived from Au ore bodies of the Yilgarn Craton: 156 from Salt Creek, 152 from Majestic, 38 from Imperial, 34 from Astro, 84 from Cosmo East, 202 from GQ and 209 from Vogue.

10.5.1. Spectrum range, right limb range, left limb range and spectrum asymmetry

The range of the singularity spectrum that quantifies a multifractal is a function of the number of individual fractal dimensions (scaling laws) that describe the dynamics of the system. A

monofractal system is one that is described by a single fractal dimension (i.e. a single scaling law value). Such an example might be a system characterized by an *aperiodic* signal that oscillates between the highest and lowest values over approximately regular intervals. Systems in which all sub-signals correlate over similar length scales and amplitudes (i.e. the signal is relatively regular and closer to periodic) will be characterized by a narrow range of singularity spectrum. Conversely, a system in which the sub-signals correlate over a diverse range of scales will be characterized by a broad singularity spectrum (a greater number of fractal dimensions). The range of the singularity system is therefore an important quantity for comparing the dynamics of signals.

The range of a singularity spectrum is sub-divided into two key components: a left limb and a right limb. The left and right limbs of a singularity spectrum describe different aspects of the system – the dynamics of the highest and lowest probability values, respectively. The highest probability values in a typical Au assay signal are the common low grades; the lowest probability grades are the rare high grades (e.g. large nuggets). Where these two components of a signal behave similarly, the singularity spectrum will be approximately symmetric (i.e. both limbs are of similar span). Where each of these components behaves differently, the singularity spectrum becomes asymmetric. Therefore, left limb width, right limb width and spectrum asymmetry are important characteristics for quantifying Au dynamics in hydrothermal systems. Here, a method for quantifying the degree of symmetry/asymmetry of a singularity spectrum is presented, allowing objective comparison. The ratio of the two limbs is acquired by dividing the broader by the narrower. Where the left hand limb is broader, the ratio is assigned as positive. This is referred to as right-handed asymmetry. Where the right hand limb is the broader, the ratio is assigned as negative. This is referred to as left-handed asymmetry. Using this system, a perfectly symmetrical spectrum has an asymmetry measure of 1 (or, equally, -1). The greater the asymmetry value deviates from this (either becoming >1 or <-1) the greater the spectrum asymmetry. A schematic illustration of standard spectrum asymmetry values is included alongside the spectrum asymmetry histograms of each ore body for reference.

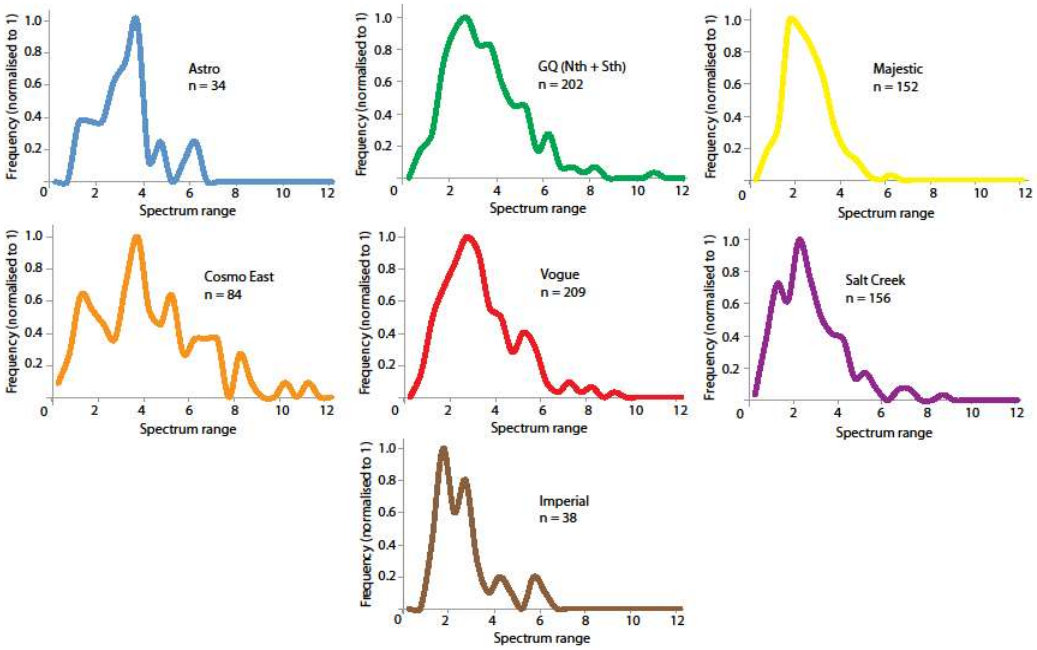

Figure 10.6. Histogram distributions of singularity spectrum ranges in each ore body. The Yindarlgooda dome ore bodies (Salt Creek, Imperial and Majestic) generally show narrower distributions in the range of singularity spectra than those from Sunrise Dam, although Astro also shows a narrow distribution. Bin width = 0.5.

Figure 10.6 shows the distributions of singularity spectrum range within each of the ore bodies. All deposits show significant internal variability in singularity spectrum range. Majestic, Imperial and Astro display the narrowest variations in spectrum range, whereas Cosmo East displays the largest. Majestic and Imperial spectrum ranges peak at 1.5 – 2, with mean ranges of 2.54 and 2.71, respectively. Salt Creek spectrum widths peak between 2 – 2.5, with a mean of 2.75. Astro and Cosmo East spectrum ranges peak between 3.5 – 4 with mean ranges of 3.24 and 4.35, respectively. Cosmo East has the most multi-modal spectrum range distribution of all the deposits. Vogue and GQ spectrum ranges peak at 2.5 - 3, with mean spectrum ranges of 3.37 and 3.49, respectively. Ore bodies in Sunrise Dam have greater proportions of spectra ≥ 2.5, higher modal peaks in spectrum range and higher mean spectrum ranges than those situated in the Yindarlgooda dome (Salt Creek and Majestic/Imperial). The greatest distinction is between Cosmo East (broad spectra) and Majestic and Imperial (narrower spectra). Combined, the 529 analyses for all lodes at Sunrise Dam have a mean singularity spectrum width of 3.54 (st. dev. 1.79), greater than those from the Yindarlgooda Dome.

Salt Creek, Majestic and Imperial display narrower distributions in left hand limb range than the ore bodies at Sunrise Dam, possessing significantly fewer with ranges ≥ 2 (Figure 10.7). Cosmo East is distinct from the other Sunrise Dam ore bodies, with a more irregular distribution and a significantly greater proportion of spectra with ranges ≥ 2.5. Salt Creek, Majestic and Imperial also display the narrowest distributions in right hand limb width (Figure 10.8) and have lower peak values than ore bodies at Sunrise Dam (Figure 10.8). Cosmo East displays a notably broader distribution than Vogue, GQ and Astro, and has the highest peak range of any ore body. Most of the ore bodies from Sunrise Dam display a preponderance of spectra with left-handed asymmetry (Figure 10.9) except Astro, which has approximately equal proportions of left and right handed. The Yindarlooda dome ore bodies (Majestic, Imperial and Salt Creek) have approximately equal proportions of left and right-handed singularity spectra.

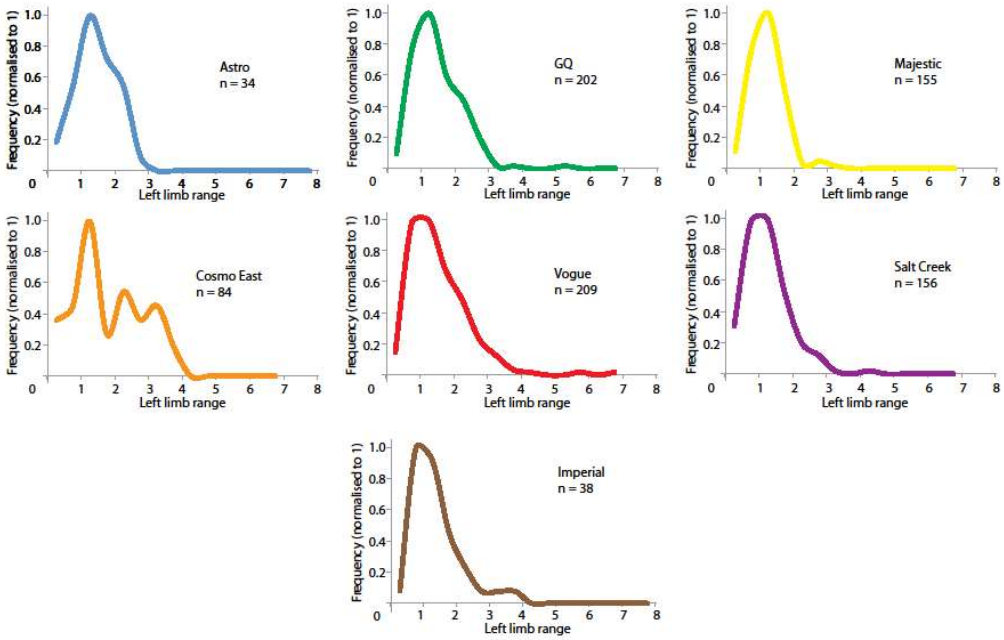

Figure 10.7. Histogram distributions of singularity spectrum left hand limb ranges for all ore bodies. Note that Salt Creek, Imperial and Majestic are the narrowest; Vogue, GQ and Astro are broader. Cosmo East distinguished from the other Sunrise Dam ore bodies. Bin width = 0.5.

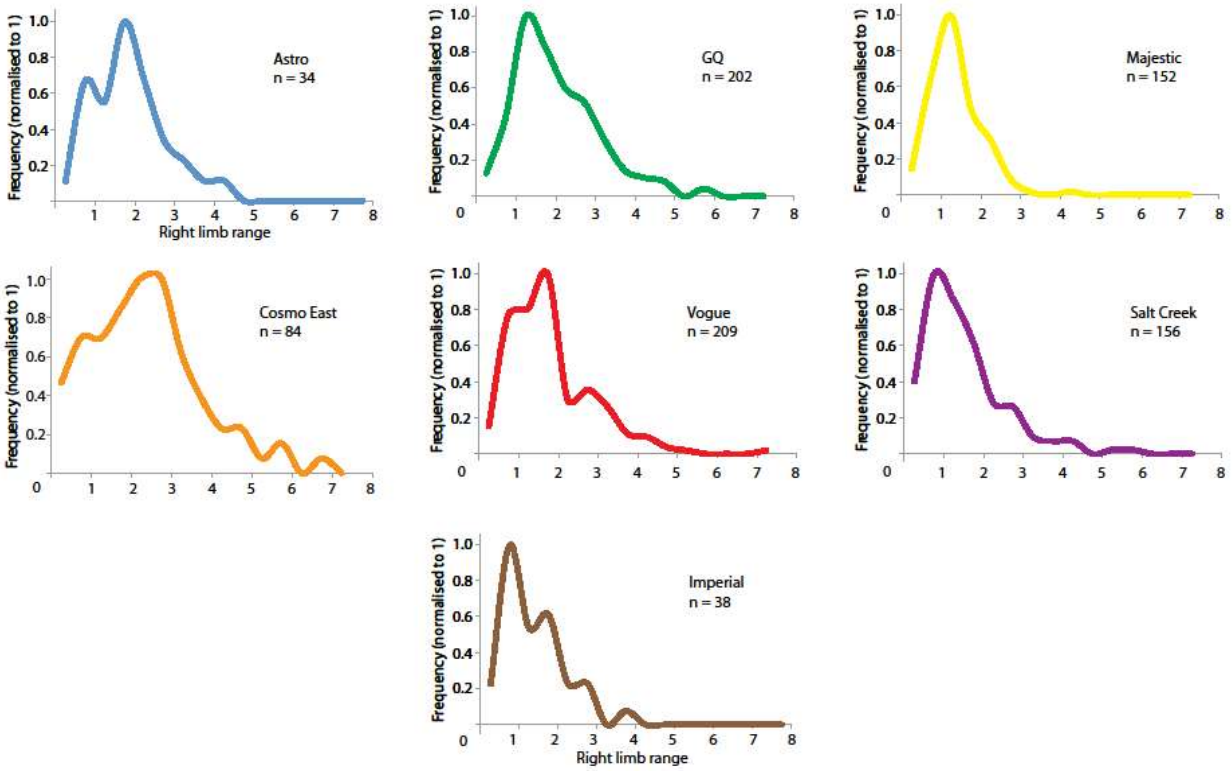

Figure 10.8. Histogram distributions of singularity spectrum right hand limbs for all ore bodies. Note that Salt Creek, Imperial and Majestic show the narrowest. Vogue, GQ and Astro have broader right limbs and broader distributions. Cosmo East is unique, with the highest mode and greatest distribution of all ore bodies. Bin width = 0.5.

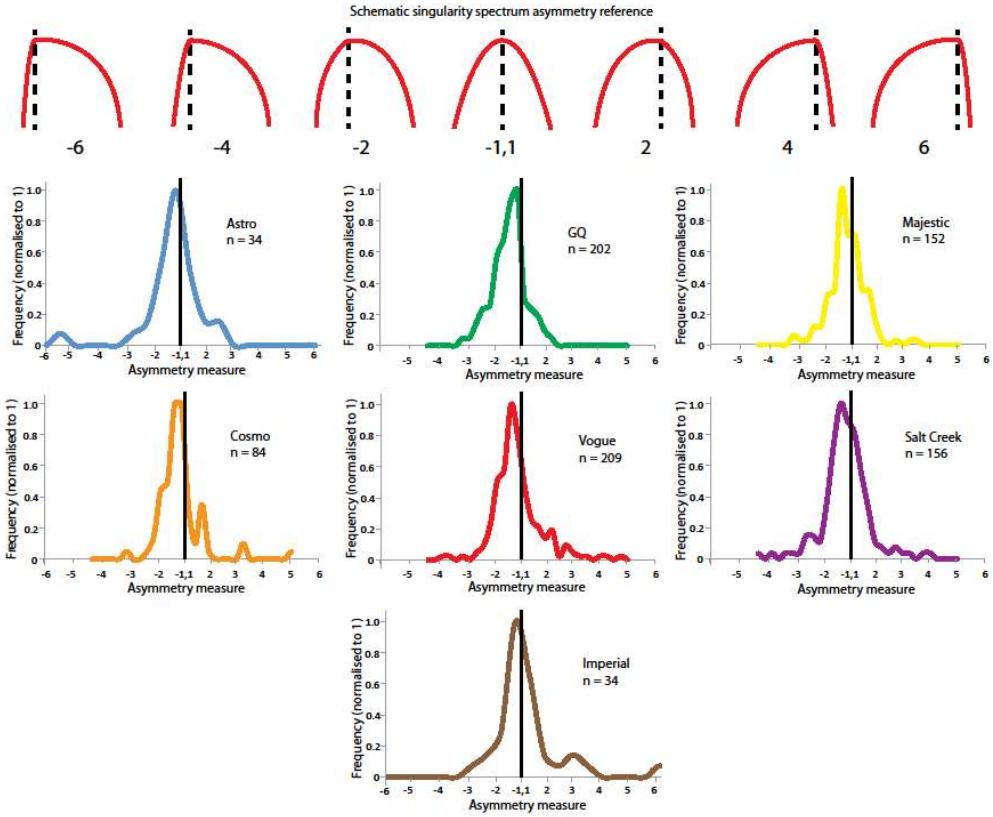

Figure 10.9. Histogram distributions of singularity spectrum asymmetry for all ore bodies. Negative values denote a

wider right hand limb; positive values denote a broader left hand limb. Sunrise Dam ore bodies show a dominance of left handed asymmetry; Majestic, Imperial and Salt Creek have approximately equal proportions of left and right-handed asymmetry. Bin width = 0.25.

10.5.2. Positions of key indices on the singularity spectrum - D0, D1, D2, D+∞ and D-∞.

In addition to ranges and asymmetries, singularity spectra may also be compared using the positions of key indices that lie on the spectrum (D0, D1, D2, D+∞ and D-∞). D0, D1, D2 are points on the spectrum defined by tangents with slopes of 0, 1 and 2, respectively. D0 (the capacity dimension) lies at the apex of the spectrum, where the left and right limbs meet. D1 and D2 are located on the left limb of the spectrum. D+∞ and *D*-∞ mark the left and right hand extremes of the spectrum, where it connects with the α-axis.

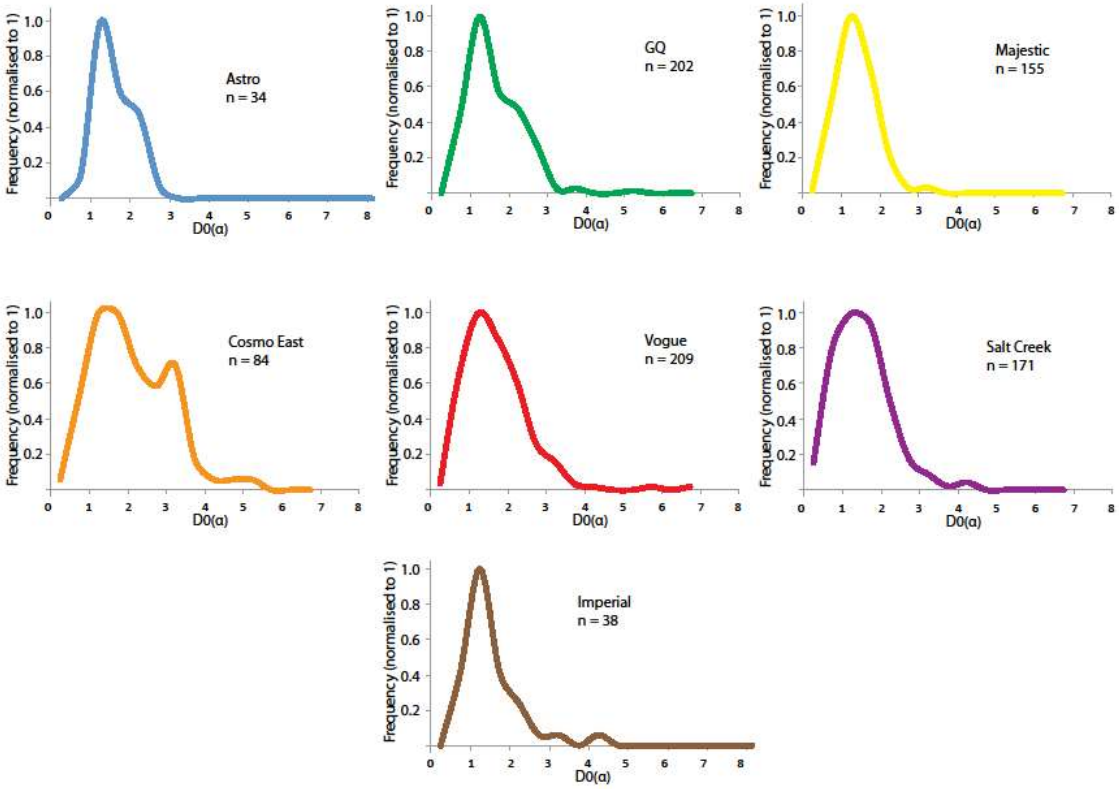

Figure 10.10. Histogram distributions of D0(alpha) values in each of the ore bodies. All ore bodies show a similar uni-modal distribution with the exception of Cosmo East, which is bi-modal. Cosmo East displays the broadest distribution, whereas Majestic and Imperial display the narrowest. Bin width = 0.5.

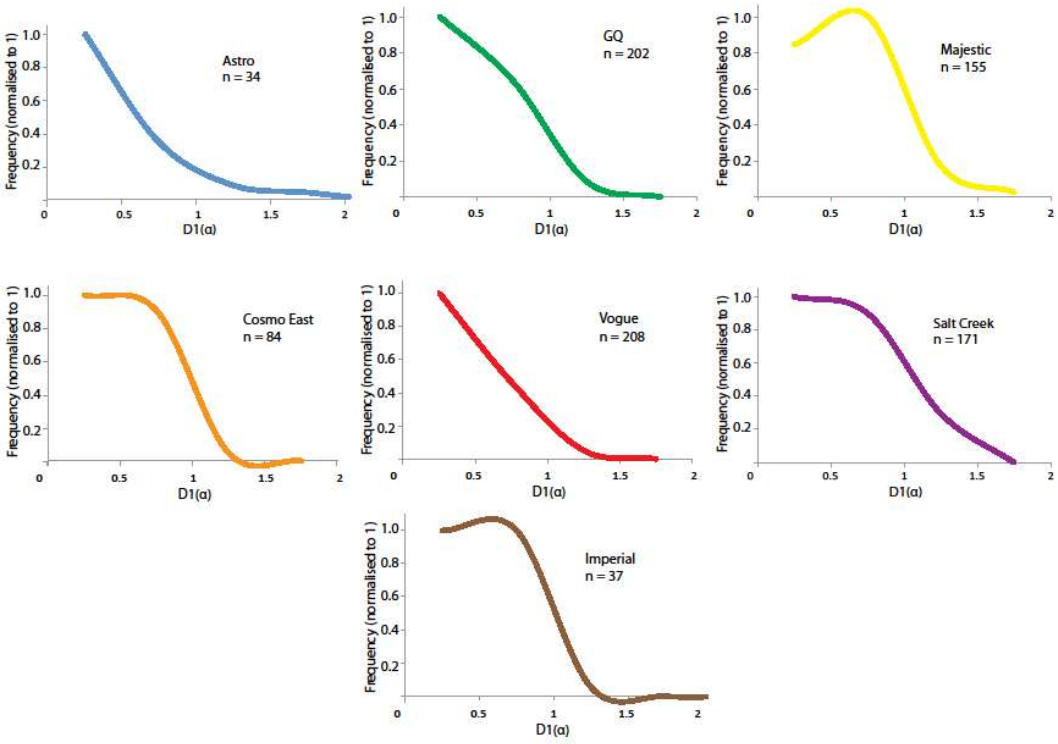

Figure 10.11. Histogram distributions of D1(alpha) values in each of the ore bodies. Vogue, GQ and Astro from Sunrise Dam display similar behaviour, peaking in the range 0-0.5. Majestic and Imperial have higher values, peaking in the range 0.5-1. Bin width = 0.5.

All ore bodies (with the exception of Cosmo East) show similar peak values and distributions in D0(α) (Figure 10.10). Cosmo East displays a higher mean, and a significantly broader profile with bi-modal distribution. D1(α) distributions in Vogue, GQ and Astro at Sunrise Dam are similar (Figure 10.11) peaking in the range 0-0.5 and smoothly declining with increasing value. Salt Creek, Majestic, Imperial and Cosmo East display greater proportions of spectra with D1(α) values extending into the range 0.5-1, which is the peak range for Majestic and Imperial. Majestic, Salt Creek and Imperial display similar D1 f(α) profiles (figure 10.12) peaking in the range 0.5-1. GQ and Vogue (Sunrise Dam) have similar D1 f(α) profiles, with high proportions in the ranges 0-0.5 and 0.5-1. The Astro and Cosmo East D1 f(α) profiles peak at 0-0.5 and decline with increasing value. All seven ore bodies display similar D2(α) and D2 f(α) profiles (Figures 10.13 and 10.14, respectively). However, Salt Creek has a higher proportion of D2(α) values greater than 0.6 (Figure 10.13). A number of singularity spectra in ore bodies from Sunrise do not have D2 values because when the left limb of a spectrum is broad the tangents to it may not reach 2. Mean D+∞ values in Majestic and Imperial are similar to those in Sunrise Dam ore bodies. Salt Creek has a marginally higher D+∞ value than the other deposits (Figure 10.15). D-∞ values in Salt Creek, Majestic and Imperial are lower than those in Sunrise Dam ore bodies. This is consistent with generally narrower singularity spectra in Salt Creek, Majestic and Imperial.

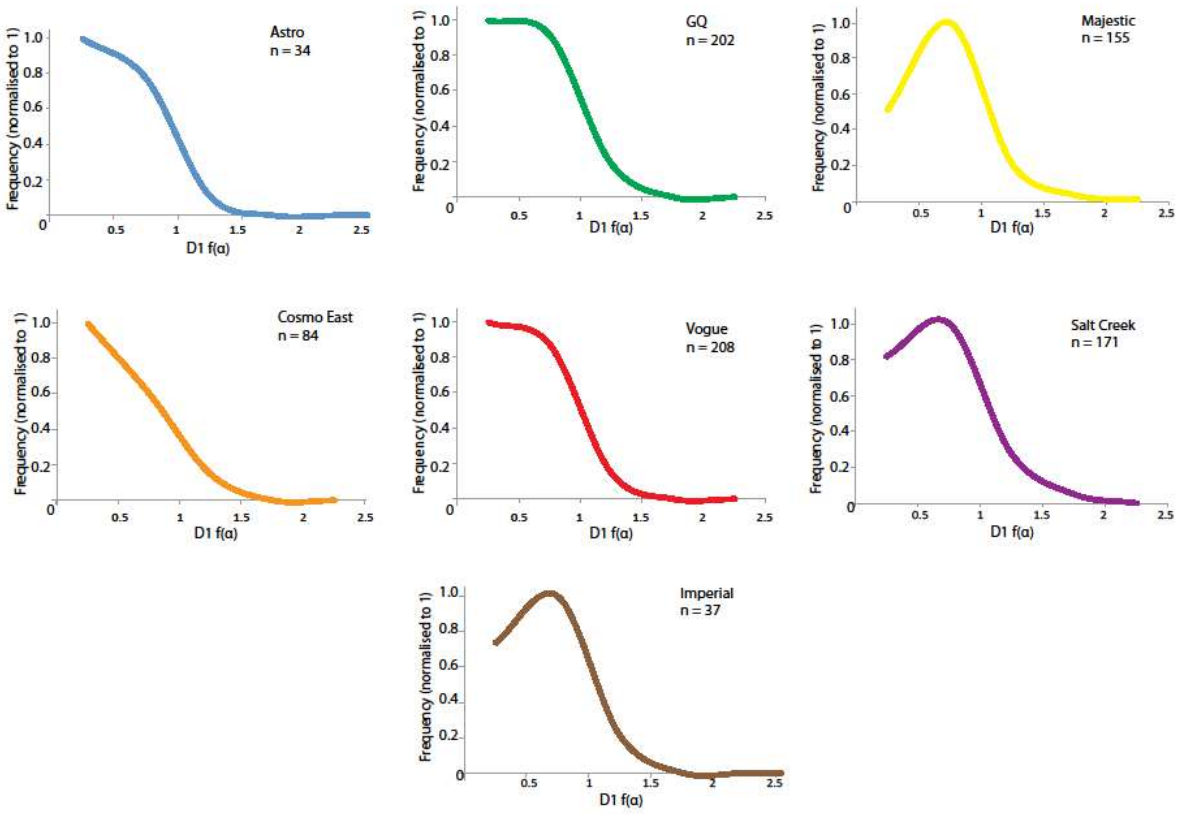

Figure 10.12. Histogram distributions of D1 (F-alpha) values in each of the ore bodies. Majestic, Salt Creek and Imperial show similar distributions, peaking in the range 0.5-1. GQ and Vogue (Sunrise Dam) exhibit similar distributions, peaking in the range 0.5-1. GQ and Vogue (Sunrise Dam) exhibit similar distributions, Astro slightly less so. Cosmo East is distinct from the other ore bodies at Sunrise Dam, showing the greatest proportion of values in the range 0-0.5 and lower proportions at higher values. Bin width = 0.5.

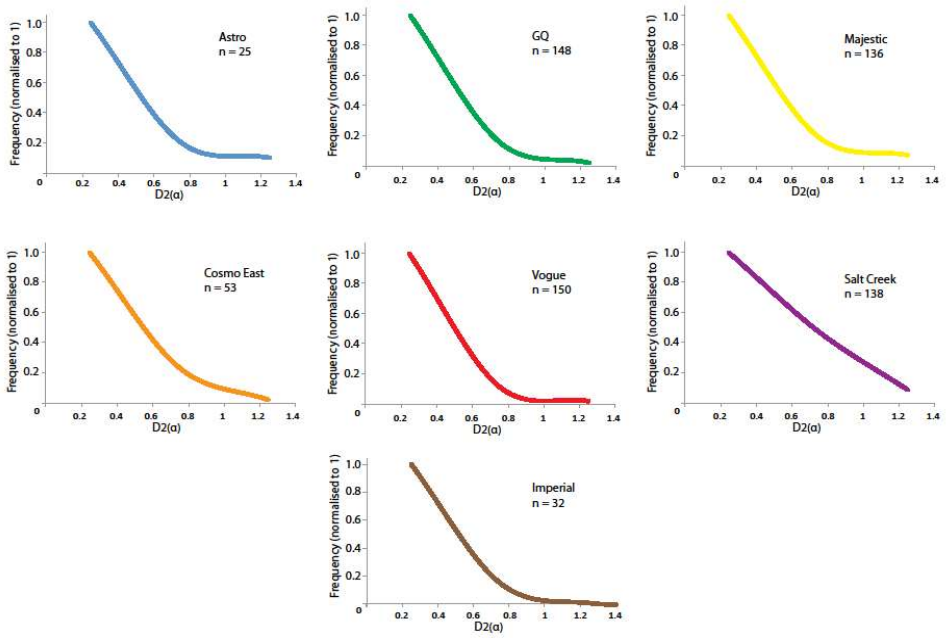

Figure 10.13. Histogram distributions of D2(alpha) values in each of the ore bodies. Six ore bodies display similar distributions; Salt Creek shows a greater proportion of spectra with higher values of D2(alpha), particularly for D2(alpha) greater than 0.6. Bin width = 0.5.

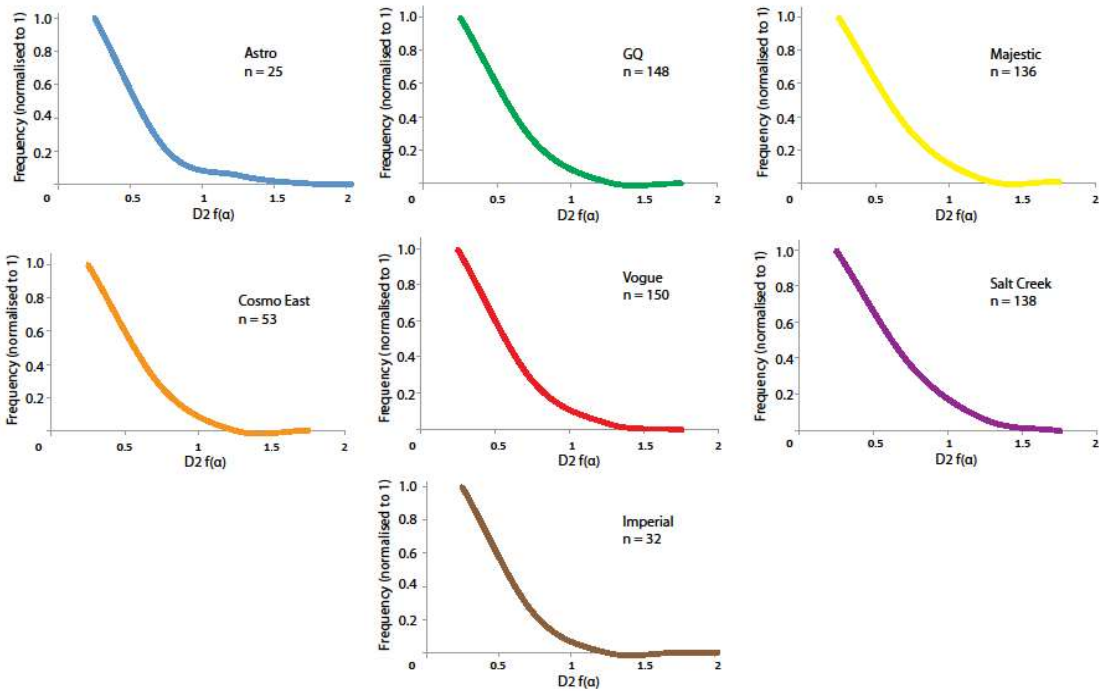

Figure 10.14. Histogram distributions of D2 (F-alpha) values in each of the ore bodies. All ore bodies show the same behaviour. Bin width = 0.5.

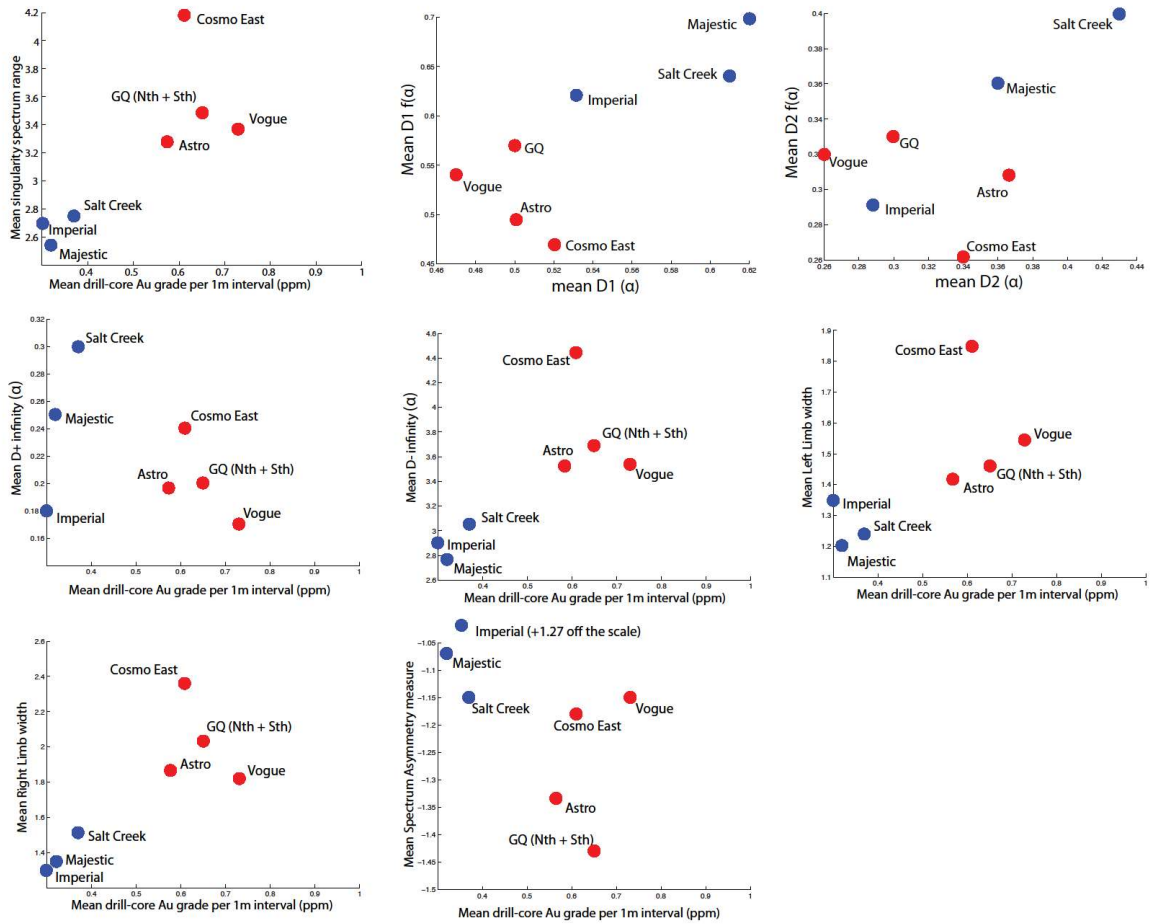

Figure 10.15. Plots of mean singularity spectrum metrics versus average Au grade for all drill core analysed from each ore body. Yindarlgooda Dome ore bodies are blue; Sunrise Dam ore bodies are red. Lower grade ore bodies from the Yindarlgooda dome (Salt Creek and Majestic) exhibit distinct signatures to those from the higher-grade Sunrise Dam ore

bodies. Cosmo East shows distinctive behaviour to other ore bodies from Sunrise Dam in a number of spectrum metrics. The higher grade ore body from the Yindarlgooda dome (Imperial) may be grouped with the lower grade ore bodies (Salt Creek and Majestic) for most metrics, but clearly groups with the Sunrise Dam ore bodies for mean D2(alpha).

10.5.3. Summary of deposit-scale non-linear dynamics in Au.

Wavelet-based analysis of Archaean hydrothermal Au ore bodies at 100m-scale demonstrates that Au organizes spatially as multifractals. Au in all seven ore bodies shows complex spatial dynamics, quantified by broad singularity spectra (broad ranges in fractal dimension). The use of multifractal singularity spectra to characterize the non-linear spatial dynamics of Au distinguishes three groups of ore body. Those from the Yindarlgooda dome (Salt Creek, Majestic and Imperial) exhibit similar signatures in many spectrum metrics (Figure 10.15) including mean singularity spectrum range. Vogue, GQ and Astro at Sunrise Dam exhibit similar signatures to one another that are distinct from those in the Yindarlgooda Dome. The Cosmo East breccia lode at Sunrise Dam further distinguishes itself from both those in the Yindarlgooda dome and the other Sunrise Dam lodes. The distinction between ore bodies in the Yindarlgooda dome and those from Sunrise Dam is also evident when mean singularity spectrum metrics are plotted versus mean drill core Au grades (Figure 10.15) and versus Au endowment for each ore body (Figure 10.16). Higher endowed deposits have broader singularity spectra, left limbs and right limbs than the lesser endowed. Higher endowed deposits generally have higher D-∞ values and stronger left-handed asymmetry. Cosmo East (lowest resource ore body at Sunrise Dam) shows distinct behaviour to the others in the system having significantly broader spectra, broader left limbs, broader right limbs and higher D-∞ values.

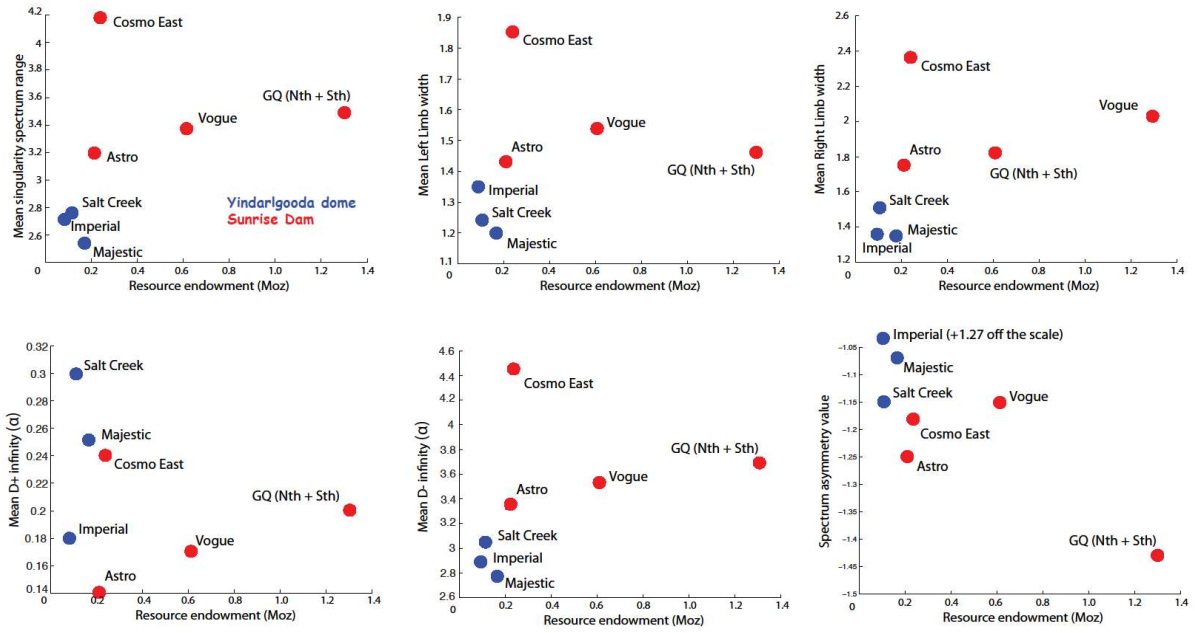

Figure 10.16. Plots of mean singularity spectrum metrics for each ore body versus its resource endowment (MOz's). Yindarlgooda Dome ore bodies are blue; Sunrise Dam ore bodies are red. Higher endowed ore bodies from Sunrise Dam show distinct signatures to lower endowed ore bodies from the Yindarlgooda dome (Salt Creek and Majestic). Resource endowments from Ellison, P., 2016. Sunrise Dam resource inventory. AGA unpublished data.

Sunrise Dam ore bodies have more complex non-linear spatial dynamics (i.e. a stronger hierarchical spatial organization) than those in the Yindarlgooda Dome. Au in Sunrise Dam is more irregularly and intermittently distributed (more nuggetty) showing greater variability in down-hole

wavelengths and amplitudes of correlation. The breccia lode (Cosmo East) shows the most extreme irregularity and intermittency of the ore bodies analysed. Therefore, Group III mineralization at Sunrise Dam, dominantly associated with D_{4a} deformation, shows distinct spatial behaviour to Group I mineralization dominantly associated with D_3 deformation. Conversely, generally narrower spectra in Majestic and Imperial suggest that Au is somewhat more regularly distributed. The high probability (low concentration) Au grades occupy the left limb of the singularity spectrum; the low probability (high concentration) Au grades occupy the right limb. Left-handed asymmetry in a singularity spectrum therefore indicates that the low grades are more regularly and uniformly distributed than the high grades, and *vice versa*. Majestic, Imperial and Salt Creek show approximately equal proportions of left and right-handed asymmetry (weak to moderate). Near symmetry in many of the drill holes shows that the low grades (left limb) and high grades (right limb) show approximately equal complexity in their wavelengths and amplitudes of correlation. Some areas of these deposits show stronger left-handed asymmetry (values $\leq$ -2), indicating that the common low concentrations of Au are more uniformly distributed than the rare high grades. Other sections show stronger right-handed asymmetry (values $\geq$ 2), indicating that the common low concentrations of Au are more irregularly and intermittently distributed than the rare high grades. The GQ, Vogue and Cosmo East ore bodies at Sunrise Dam show greater proportions of left-handed asymmetry (weak to moderate). These ore bodies are therefore characterized by more regularly distributed low Au grades and more irregularly distributed high grades.

10.6. Relations of singularity spectra to rock lithology and drill core orientation.

10.6.1. Non-linear dynamics of Au classified by dominant host rock lithology.

Au mineralization in Salt Creek is almost exclusively confined to within the Magnetite-Quartz-dolerite and leucodolerite of Unit III (Figure 10.5) and so drill hole intersections cannot be lithologically separated. Mineralization in Majestic and Imperial is hosted within a lithologically homogeneous (weakly) porphyritic quartz-diorite stock. Drill cores in the Astro ore body at Sunrise Dam are dominated by dolerite and gabbro (many exclusively) with four exceptions dominated by volcaniclastic sandstone. The other ore bodies at Sunrise Dam (Vogue, GQ and Astro) show greater diversity in host rock lithology. Drill cores in each of these ore bodies were therefore classified according to dominant host rock lithology to evaluate variations in the non-linear dynamics of Au between them. Dominant lithologies are defined as those composing the greatest proportion of the drill core interval.

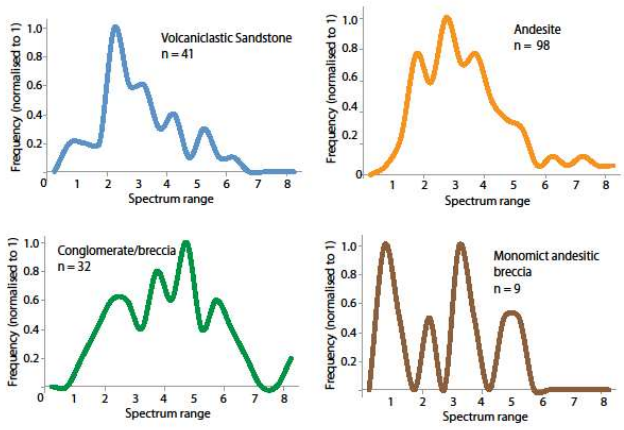

Figure 10.17. Singularity spectra widths for Au in GQ classified by the dominant host rock lithology over the drill core

interval (volcaniclastic sandstone, andesite, conglomerate/breccia and monomict andesitic breccia).

Drill cores in GQ were classified into those dominated by volcaniclastic sandstone, andesite, polymictic conglomerate/breccia or monomictic jigsaw-fit andesitic breccia (Figure 10.17). Au in all four lithologies in GQ shows broad variability in singularity spectrum width, with narrow end-members between 0 – 1 and broad end-members between ~6 - 7.5. Conglomerate/breccia-dominated Au has the most evenly distributed profile across this range. Most Au spectra in andesite-dominated sections of GQ lie between ~1.5 – 5. Au in volcaniclastic sandstone-dominated sections of GQ shows significantly narrower singularity spectra than other lithologies, with ranges dominantly between 2 – 3.5. Therefore, Au in volcaniclastic sandstone-dominated sections is more regularly distributed and less nuggetty than that within other dominant lithologies in GQ. By contrast, Au within conglomerate/breccia-dominated sections of GQ is more intermittently distributed with a stronger hierarchical spatial organization. The multi-modal frequency distribution of Au singularity spectra ranges in intervals dominated by monomict andesitic breccia (Figure 10.17) is a function of fewer data points (n) for the lithology. If more data was available, the present gaps would likely also be occupied by intermediate values. Therefore, the range between end-member spectrum widths in the monomict breccia category is more informative than its multi-modality.

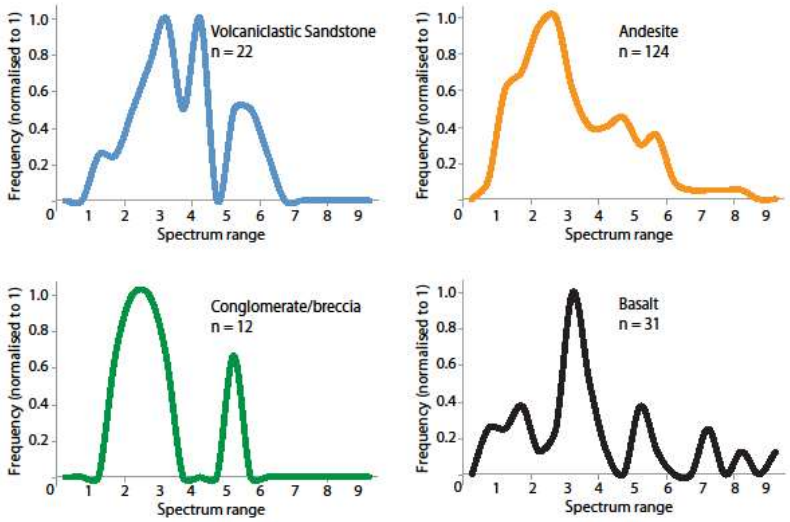

Figure 10.18. Singularity spectra widths for Au in Vogue classified by the dominant host rock lithology over the drill core interval (volcaniclastic sandstone, andesite, conglomerate/breccia and basalt).

Drill cores in Vogue were classified into those dominated by volcaniclastic sandstone, andesite, polymictic conglomerate/breccia or basalt (Figure 10.18). Au in volcaniclastic sandstone and conglomerate/breccia-dominated sections of Vogue shows singularity spectrum ranges between 1 – ~6. Au in basalt and andesite-dominated sections of Vogue show spectrum ranges extending from narrow (0 – 1) to extremely broad (8.5 – 9.5). Au in andesite and conglomerate/breccia-dominated sections show the greatest proportions of narrow spectra (~1 – 3.5). Modal peaks in spectrum range in basalt and volcaniclastic sandstone-dominated sections of Vogue are higher than in other lithologies (2.5 – 4 and 2.5 – 4.5, respectively).

Drill cores in Cosmo East were classified into those dominated by volcaniclastic sandstone, andesite, polymictic conglomerate/breccia, basalt or porphyritic andesite (Figure 10.19). Au singularity spectrum width profiles for all lithologies in Cosmo East are more strongly multi-modal

than in GQ and Vogue. Au in volcaniclastic sandstone, andesite and basalt-dominated sections of Cosmo East are highly variable, with end-members extending from very narrow (~0 – 1) to extremely broad (8.5 – 10). Singularity spectra in volcaniclastic sandstone and basalt-dominated sections peak in the range 3 – 6. Singularity spectra in andesite-dominated sections of Cosmo East have two peaks of equal strength at ~2 – 3 and ~ 5 – 6. Au spectrum ranges in porphyritic andesite span between 1 – 7, with three peaks of equal strength. Au hosted in sections of Cosmo East dominated by conglomerate/breccia is distinct from the other lithologies, having the narrowest singularity spectra (ranging between 0.5 – 5). Au in conglomerate/breccia-dominated sections is therefore more regularly distributed than in other lithologies, in which it is more nuggetty and intermittent.

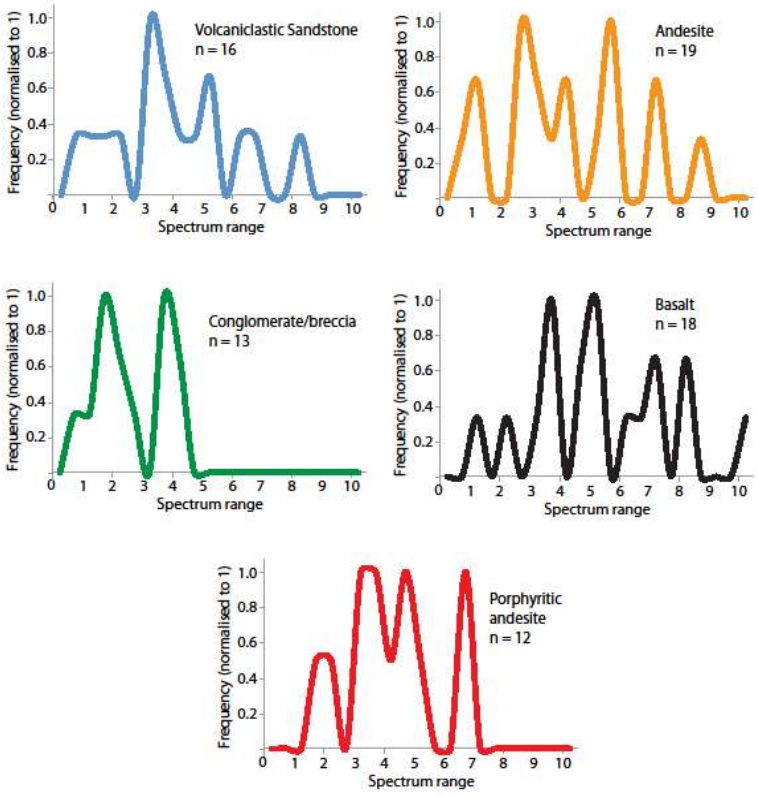

Figure 10.19. Singularity spectra widths for Au in Cosmo East classified by the dominant host rock lithology over the drill core interval (volcaniclastic sandstone, andesite, conglomerate/breccia, basalt and porphyritic andesite).

10.6.2. Non-linear dynamics of Au classified by drill core orientation.

Drill cores in Majestic and Imperial consistently plunge ~60° due east, providing strong directional control upon the singularity spectrum signatures. Drill cores through Salt Creek are also consistently oriented, plunging ~60° due northeast. Drill cores through the Sunrise Dam ore bodies are variably oriented, except Cosmo East – which has plunges shallowly to the east-northeast (0 - 35°) and west-southwest (0 - 10°).

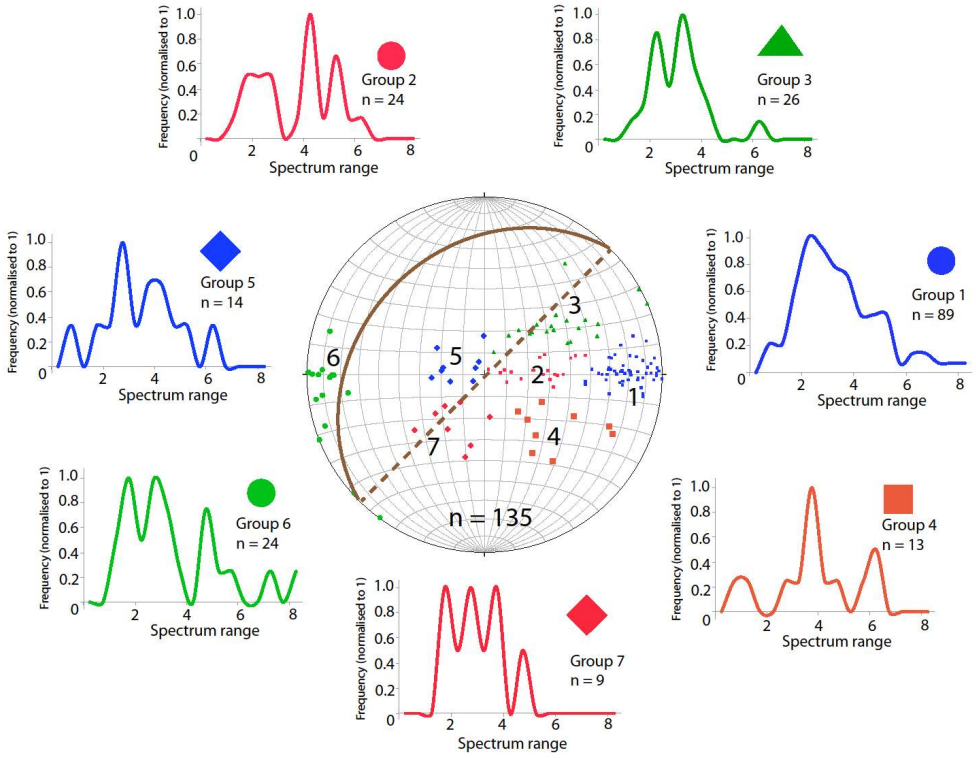

Figure 10.20. Stereonet displaying the orientations of drill cores through the GQ ore body at Sunrise Dam. Drill cores are sub-divided into 7 groups according to orientation, each marked using a different symbol and with group numbers marked on the stereonet. The plane indicates the orientation of the major gently to moderately northwest-dipping shear zones (e.g. Sunrise, Mako, Midway) that define the Group 1 ore bodies such as GQ. Dashed line marks the strike of the shear zones. Frequency-normalized histograms of the Au singularity spectrum widths within each group are presented around the stereonet.

Drill cores through the GQ ore body at Sunrise Dam are highly variable in orientation. They were therefore categorized into seven groups based on orientation. Figure 10.20 shows the orientations of the seven groups on a stereonet, with the distributions of spectrum range within each presented as frequency histograms. Also marked is the orientation of the moderately northwest-dipping shear zones that define Group 1 ore bodies such as GQ (e.g. Sunrise, Mako, and Midway). Groups 3 and 7 are moderately plunging and have trends close to the strike of the shear zones. Au singularity spectra in these two groups are generally narrow, with restricted distributions primarily between ~ 1 – 4.5. Drill cores in the other five groups trend at greater angles to shear zone strike. Group 5 drill cores trend approximately parallel to shear zone dip, but plunge more steeply than it. Group 4 drill cores plunge moderately to the southeast - approximately perpendicular to shear zone orientation. Au singularity spectra in these other five groups have higher mean ranges, and show greater variability, than those in groups 3 and 7. Au in GQ is therefore more regularly distributed when measured in drill cores with trends closer to strike of the shear zones. Au measured in orientations at higher angles to strike shows greater variability in spatial behaviour, and is generally more irregular and intermittent.

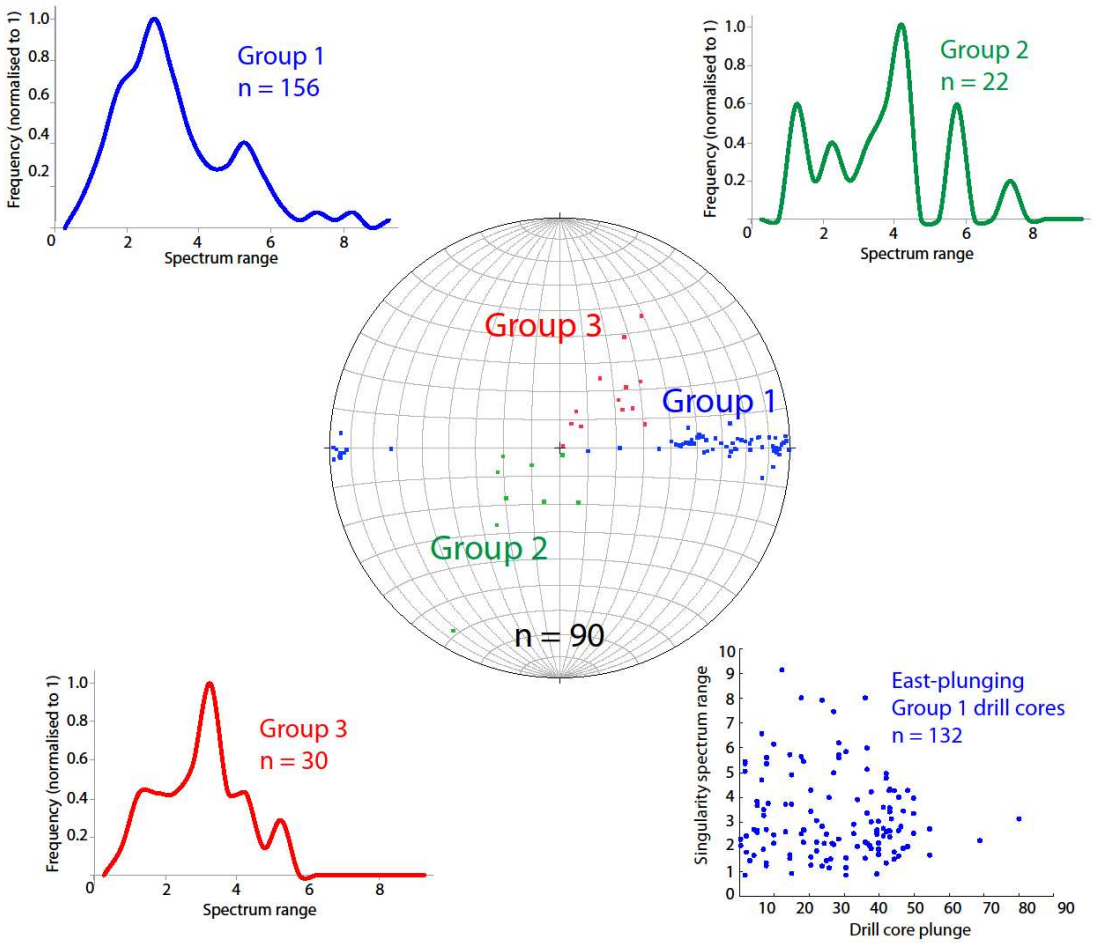

Figure 10.21. Stereonet showing the orientations of drill cores through the Vogue ore body at Sunrise Dam. Drill cores are sub-divided into 3 groups according to orientation, each marked by a different symbol and with group numbers marked on the stereonet. Frequency-normalized histograms of the Au singularity spectrum widths within each group are presented around the stereonet. The scatter plot in the lower right corner compares the plunge of each drill core in the linear array in Group 1 versus its singularity spectrum width. Note the lack of correlation between plunge and spectrum width.

Drill cores in Vogue at Sunrise Dam were sub-divided into three groups (Figure 10.21): east-west trending (Group 1), steeply south to west trending (Group 2) and north-northeast – east-northeast trending (Group 3). Au in east-west trending drill cores shows the greatest proportion of narrow singularity spectra ranging between 0.5 – 4. Therefore, Au measured in east-west trending drill cores in Vogue is more regularly distributed than that measured in other orientations. The east-west trending drill cores range from steeply east-plunging to shallowly west-plunging. Plotting eastward-plunges versus singularity spectrum width shows that narrow spectra end-members start to dominate in steeply plunging drill cores; broad spectra end-members start to dominate in more shallowly plunging drill cores. Au in north-northeast – east-northeast trending drill cores shows a modal peak in spectrum width that is slightly higher than those in east-west trending drill cores. Au in south to west-plunging drill cores shows the most variable singularity spectrum ranges and the greatest modal peak of the three groups. Au measured in these orientations is therefore the most intermittent and nuggetty.

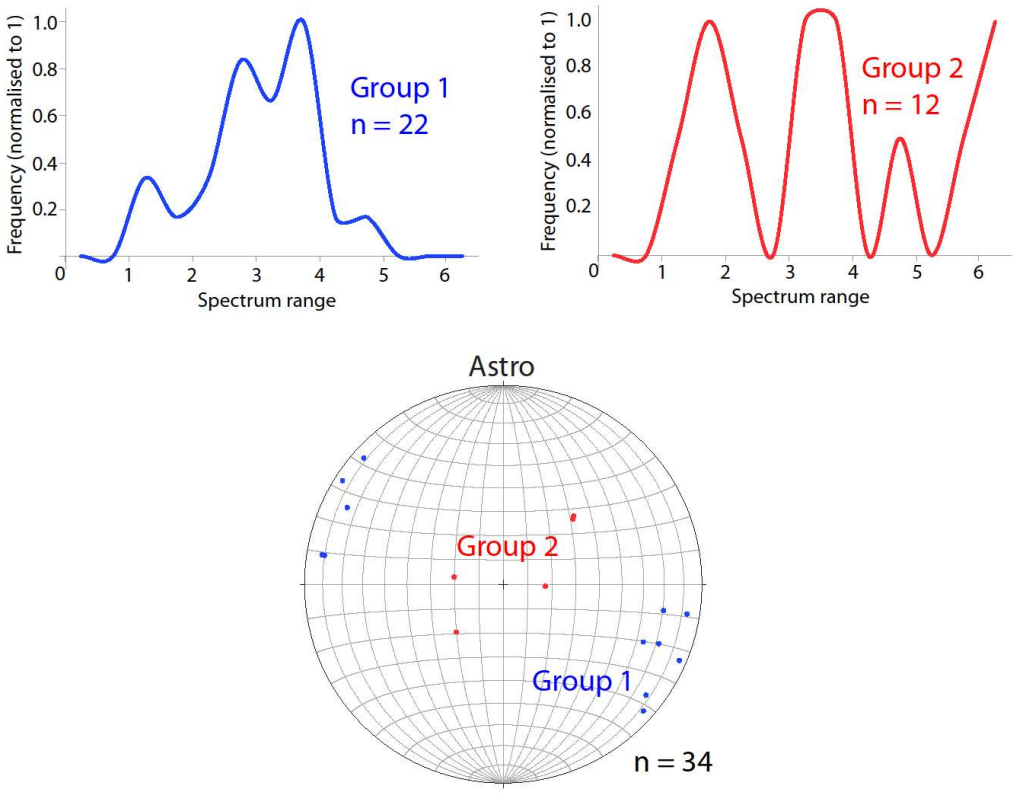

Figure 10.22. Stereonet showing the orientations of drill cores through the Astro ore body at Sunrise Dam. Drill cores are sub-divided into 2 groups according to orientation – shallowly plunging and steeply plunging. Frequency-normalized histograms of the Au singularity spectrum widths within both groups are presented next to the stereonet.

Drill core orientations in Astro may be classified into two groups (Figure 10.22): shallowly ~ east-southwest to west-northwest plunging (Group 1), and steeply plunging (Group 2). Au singularity spectrum ranges in shallowly plunging drill cores are dominantly between 2 – 4, with few end-members out-with this range. Au singularity spectra in steeply plunging drill cores are highly variable (multi-modal) and have a greater proportion of narrow spectra between ~ 1 – 2.5.

Diverse singularity spectrum widths in a range of orientations through the GQ, Vogue and Astro ore bodies at Sunrise Dam demonstrate that Au has strong variability in spatial organization (irregularity and intermittency) in three dimensions. Au analysed in drill cores trending close to strike of the main shear zones in GQ is more regularly distributed than when analysed in orientations at higher angles to strike.

10.7. Evolution of the multifractal signal in a hypothetical ore body.

Figure 10.23 demonstrates the evolution of a singularity spectrum signature for a drill hole through a hypothetical hydrothermal Au system during its deformation and mineralization history. This system experienced three distinct phases of fluid-rock interaction, each associated with different grades and spatial distribution of Au precipitation. Stage I was associated with the dissemination of low Au grades (0-0.1ppm) throughout the host rock within this section of the drill core interval. The distribution of Stage I Au is characterized by a relatively narrow singularity spectrum because it is regularly distributed across the drill hole over approximately similar amplitudes and wavelengths. Stage II deformation and mineralization produced vein-hosted Au

nuggets contained almost exclusively within veining of approximately 10-20m spacing; resulting in locally elevated grades (1.5 – 4.5ppm) that correlate over greater wavelengths within the system. Stage III deformation was highly localized, associated with metre-wide zones of intense brecciation and the precipitation of very high gold concentrations (here 54.3 and 77.3ppm) within the encasing breccia cements. Combined, the effects of these three mineralizing stages produce a three-tier hierarchical organization in Au grades, characterized by a strong (broad) multifractal signature that is analogous in range to a large number of well-endowed drill holes in the Yindarlgooda dome and Sunrise Dam ore bodies. As each mineralizing stage (of different grade and spatial wavelength) is superimposed upon the previous signal, the range of the singularity spectrum that characterizes the drill hole increases as the signal becomes more strongly multifractal.

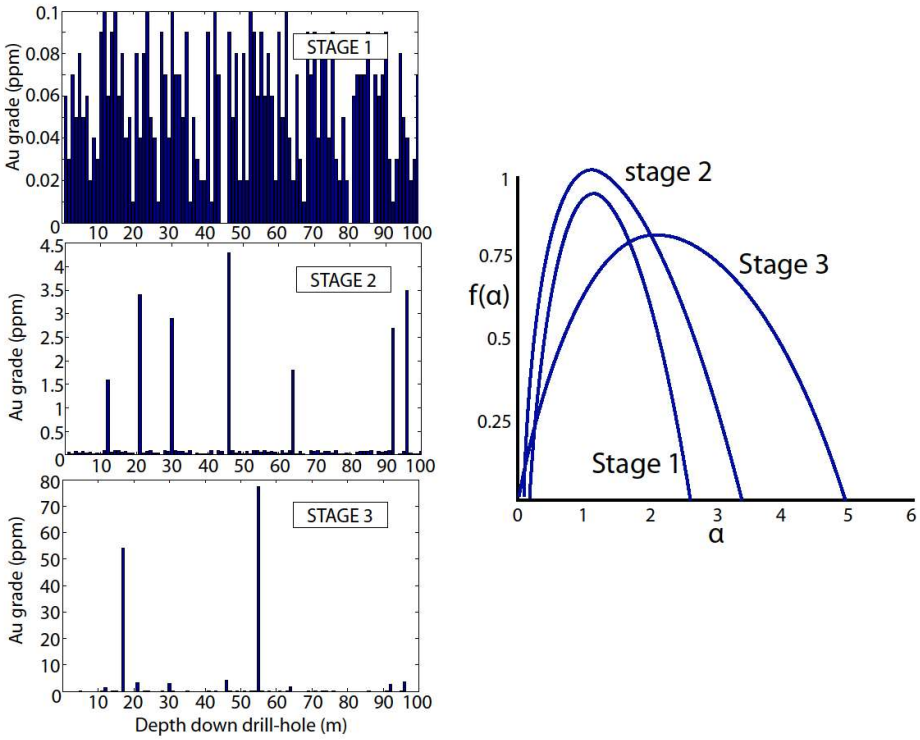

Figure 10.23. The evolution of a Au assay signal, and associated multifractal singularity spectra, through the time evolution of a hypothetical hydrothermal system. (a) Widespread deposit-scale dissemination of low-grade Au during Stage I mineralization. (b) Higher-grade, lower wavelength, Au correlations resulting from nugget precipitation in 10-20m spaced Stage II veins and shear zones. (c) Localized Stage III brecciation precipitating very high Au grades in the cements of two localized, metre-wide, zones of intense brecciation. (d) The singularity spectra for the Au assay signal following each stage of mineralization. Observe the progressive widening in range of the singularity spectrum as each spatial wavelength and Au assay 'tier' is superimposed upon previous events. The final spectrum following Stage III has a similar range to that of Au from many 100m-interval drill holes in the ore bodies examined.

10.8. The influence of rare high-grade interceptions.

Isolated high Au grade peaks are a common feature in hydrothermal systems - representing either large individual nuggets or a site of more concentrated Au deposition in veins. The influence of rare high-grade peaks upon the singularity spectrum is evaluated using drill holes MB024 and IMRC031 from the Majestic deposit. Au in both of these signals has typical background Au concentrations in the order of 0.02 – 0.1ppm. IMRC031 has a single very high concentration peak at

84.57ppm (Figure 10.24), whereas IMD024 has 3 higher concentration peaks at 4.23, 4.29 and 3.56ppm (Figure 10.25).

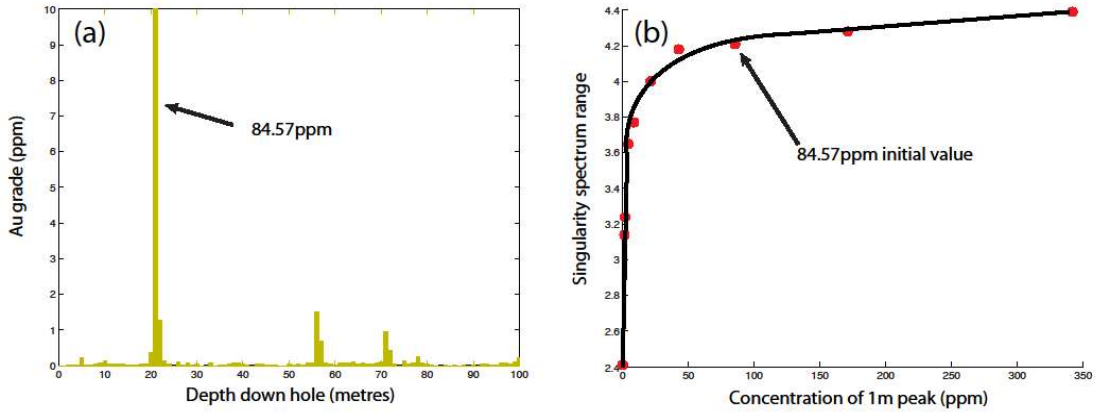

Figure 10.24. (a) The original down-hole Au assay signal for drill core IMRC031 from Majestic. The high concentration peak has a value of 84.57ppm, however the plot is capped at 10ppm to allow visualisation of the rest of signal. The concentration of the high-grade peak was progressively increased and decreased to evaluate the effect of the high-grade nugget upon the singularity spectrum over a range of values between 0.02 – 342ppm. The rest of the drill core signal was kept constant. (b) Scatter plot of how the singularity spectrum range for drill core IMRC031 varies as a function of high-grade peak concentration. Progressively reduced down to a background concentration of 0.02ppm, the singularity spectrum reduces from its initial range of 4.21 down to 2.41. Progressively increasing the concentration to 342ppm results in an increase in spectrum range that tends towards a limit at ~4.4.

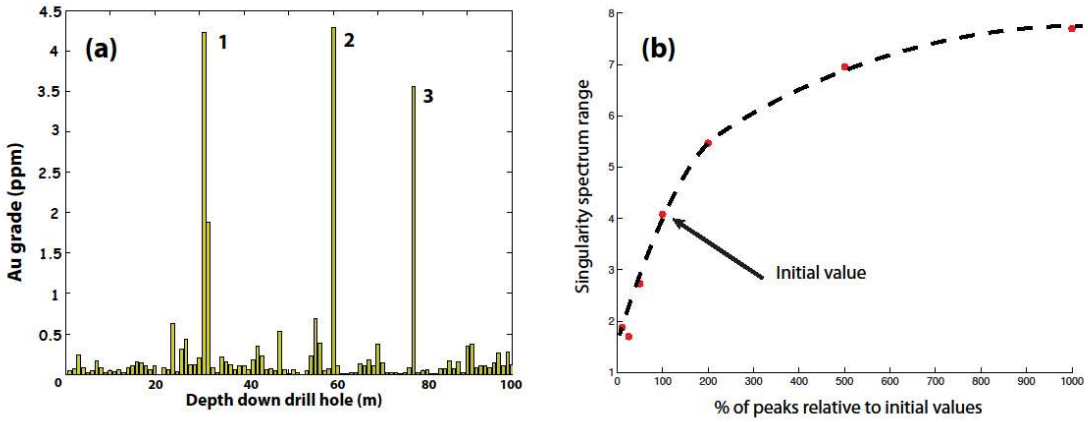

Figure 10.25. (a) The original down-hole Au assay signal for drill core IMD024 from Majestic. The concentrations of the 3 higher-grade peaks were systematically varied relative to the rest of the signal, maintaining them proportional to each other. (b) Scatter plot showing how the singularity spectra for interval varies as a function of the concentrations of the high grade peaks (expressed as a percentage of their initial values). Note the progressive reduction in spectrum range from 4.08 to 1.88 when the peaks are progressively decreased to 10% of their initial values. Progressive increase in the relative percentage of the 3 peaks results in an increase in spectrum range, tending towards an upper limit.

The high-grade (84.57ppm) peak in IMRC031 was progressively varied across a range of values between a low background concentration of 0.02pm to a high of 342ppm (4x the original concentration). The rest of signal was kept constant to evaluate the impact of the nugget upon the singularity spectrum. Progressively reducing the grade to a background concentration of 0.02ppm resulted in a progressive reduction in singularity spectrum range from an initial 4.21 down to 2.41. Progressively increasing the grade resulted in an increase in spectrum range that tends towards a limit at ~4.4. The concentrations of the 3 high-grade peaks in MB024 were also progressively varied

across a range of values from 10% - 1000% of their initial values, maintaining their values proportionate to one another. A spectrum range of 4.1 characterizes the initial dataset. Progressively reducing the values of the peaks down to 10% of their initial values results in a progressive reduction in spectrum range down to 1.88. Progressively increasing the relative percentage of the three peaks produces an increase in spectrum range, tending towards a limit at ~7.5.

Similar responses occur when the concentrations of rare high grades are modified in key drill core intervals from Cosmo East and GQ in Sunrise Dam. These observations are important as they demonstrate the importance of the concentration of rare Au grades *relative to* the frequent, high probability, grades - even where one solitary high-grade nugget is present. Importantly, the spectrum-enhancing effect of select high grades has been shown to reach an upper limit. Additionally, reduction of one of the peaks in IMD042 to background concentration while maintaining the strength of the others leads to a less pronounced reduction in spectrum range than when reducing all three. Therefore, both the concentration and number of high-grade concentrations are important contributing factors to the strength of multifractality in Au signals.

10.9. Comparing singularity spectrum metrics versus down-hole Au assay statistics.

Key singularity spectrum metrics for each drill hole were compared against down-hole Au assay data characteristics for the hole such as maximum, mean and mode gold grades. This was carried out for all seven ore bodies. In all ore bodies, spectrum range, right limb range, left limb range and spectrum asymmetry showed no correlation with Au assay statistics. A series of examples for Salt Creek is presented in figure 10.26. Key spectrum indices (D0, D1, D2, $D+\infty$, and $D-\infty$) also showed no correlation with Au assay statistics in each ore body. The lack of correlation between individual spectrum attributes and Au assay features in all ore bodies is important because it demonstrates that the singularity spectrum takes into account a variety of Au signal characteristics. Solitary high-grade nuggets have been shown to markedly enhance singularity spectrum range in some samples. However, other samples with high maximum Au grades also correspond with narrow spectra. Narrow spectra in these cases will either represent 1) relatively similar scaling dynamics in both the high and low grade concentrations, or 2) fewer concentration 'tiers' in the hierarchical organization. Conversely, broad singularity spectra may correspond to intervals with very low maximum Au grades. Au in these signals is often associated with a large number of concentration 'tiers', or atypically low background concentrations that increase the contrast in *relative* concentration between the maximum and minimum grades.

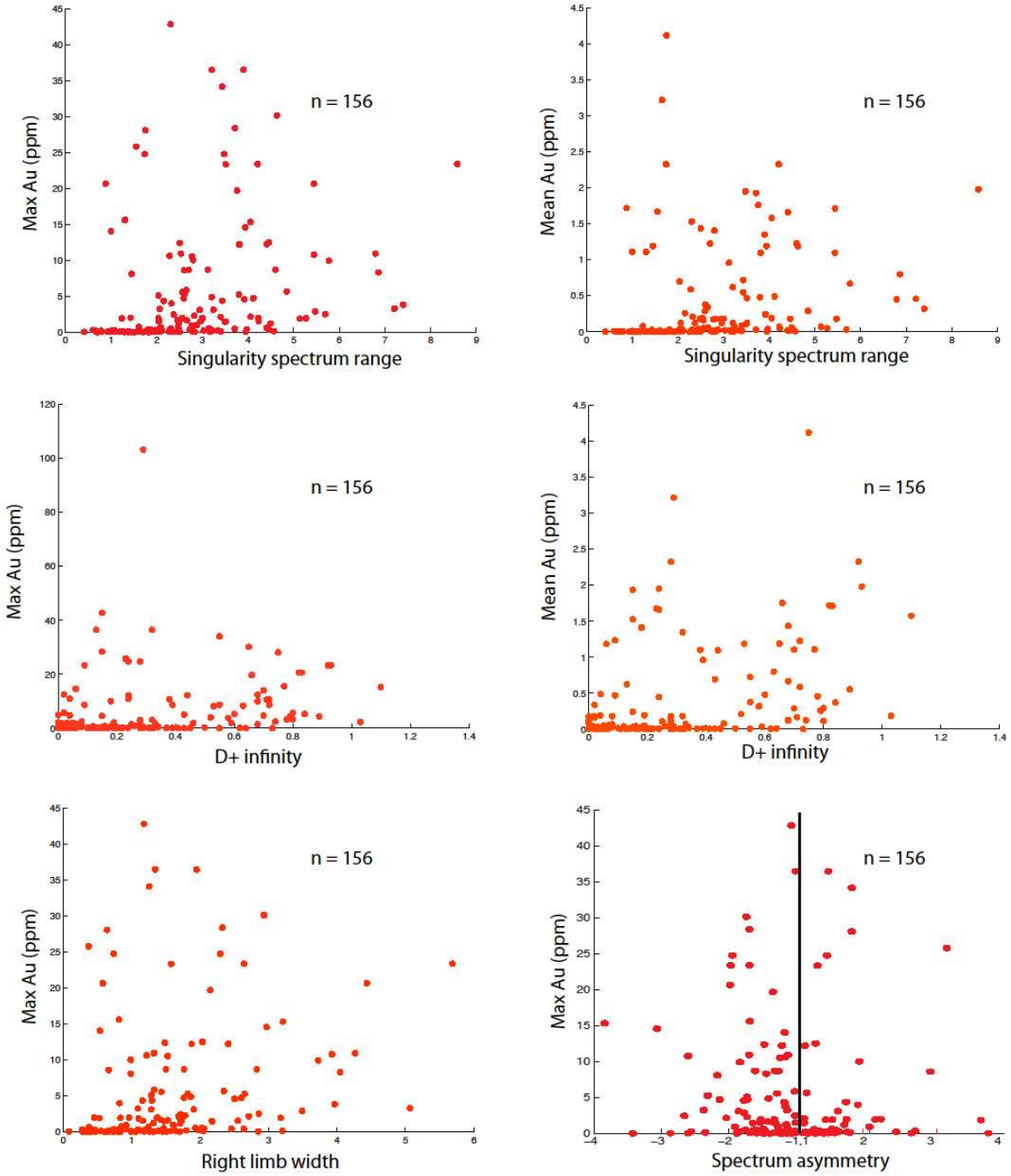

Figure 10.26. Plots of key singularity spectrum attributes from Salt Creek vs. the mean and max Au grade (ppm) for the interval. Note the lack of correlation between spectrum attributes and Au assay statistics.

Therefore, a recipe for producing broad singularity spectrum in Au is:

1) the presence of high grade nuggets (enhances concentration contrast)
2) low relative background concentrations (enhances concentration contrast)
3) larger number of concentration 'tiers' in between the maximum and minimum grades (greater variation in the amplitudes of fluctuations)
4) different wavelengths of correlation between the high and low grade concentrations

Conversely, where the inverse of these criteria are true, singularity spectra will be narrow and the signal relatively regular and uniform in its dynamics.

10.10. The effects of supergene enrichment and regolith profiles upon the multifractal signature of hydrothermal Au systems: Insights from the Majestic prospect.

10.10.1. Secondary enrichment in Au systems: Overview.

Hydrothermal, epithermal and orogenic Au systems exposed near the surface of the crust are subject to oxidation along with the host rocks, due to interaction with percolating meteoric fluids. These effects are more compounded in warm to tropical climates, such as those in Western Australia, where strong lateritic weathering occurs – rendering near-surface meteoric fluid acidic (pH typically < 5) and readily oxidizing. Coupled with high Eh (the reduction potential of a chemical species), and the production of Cl^- ions, Au may be preferentially dissolved at shallow depths above the water table to form $AuCl^-_4$. As Au-leaching fluids descend, they encounter more reducing conditions; resulting in a reduction in Eh, and consequently Au solubility. Secondary (re-)precipitation of Au in these systems therefore commonly occurs as narrow high grade zone just below the water table via reactions such as:

$$AuCl^-_4 + 3Fe^{2+} + 6H_2O \rightarrow Au + 3FeOOH + 4Cl^- + 9H^+$$

These narrow zones of secondary enrichment often represent the highest local mineralization grades within a deposit, with re-precipitated Au commonly forming large nuggets. They may also augment Au grades such that initially uneconomic lodes may be subsequently rendered economically viable. In such environments, Au deposits are sub-classified into the hypogene zone (the primary zone preserving the initial textures of deposit formation) and the overlying supergene zone (influenced by feedback mechanisms between oxidation and reduction). Further, zones of supergene enrichment are commonly spatially more extensive than the underlying primary hypogene system, therefore serving as important targeting and vectoring tools to proximate mineralized zones within the crust.

Secondary supergene processes impact the relative concentrations and spatial distribution of Au within a deposit via two fundamental mechanisms:

1) The breakdown and elimination of surrounding, more chemically-susceptible, materials and mineral species; resulting in a local relative enrichment in residual Au
2) The mesoscopic-scale dissolution, remobilization and re-precipitation of the Au itself (free Au, and that liberated from sulphide lattices); resulting in a local relative depletion, and proximate relative enhancement, in concentration

These processes result in the eradication of the primary ore-forming textures. The dissolution and leaching of Au during mechanism (2) commonly renders the uppermost section of many ore deposits barren.

10.10.2. Supergene processes at Majestic.

All drill core from the Sunrise Dam ore bodies (GQ, Vogue, Cosmo East and Astro) and the 100m interval length datasets for the Yindarlgooda dome (Imperial, Majestic and Salt Creek) were extracted from consolidated fresh bedrock below the regolith profile. This project therefore primarily investigates the hypogene (primary) sections of these Yilgarn Au systems. However, the Majestic prospect is characterized by a 1-10m thick supergene Au horizon, developed at the saprolite to fresh rock contact at depths between 30-60m (Figure 10.27). The supergene horizon presents

elevated Au grades above 0.5g/t, but typically less than 2g/t, producing a much larger footprint that extends up to 100m away from the primary mineralization system (e.g. Figure 10.28). Highest grades in the horizon are developed above the primary ore body. Above the enriched horizon, which is delineated by a presence of chrysocolla (copper oxide), the overlying rocks are strongly depleted in both Au and Cu (the latter reduced from grades of ~10,000ppm to 3-500ppm).

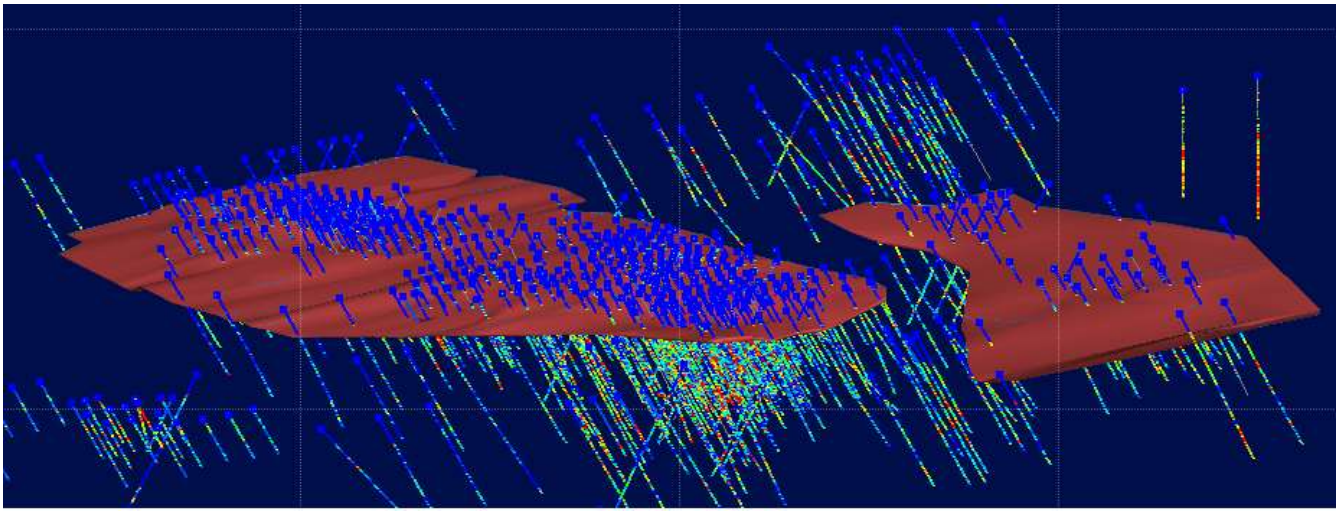

Figure 10.27. Leapfrog model showing the drill-core array at Majestic, plunging ~60° due east. Red shell surface represents the position of the narrow supergene enrichment zone, situated at depths between 30-60m. Supergene blanket is approximately sub-horizontal. Viewing perspective is 21° -> 007 (due N).

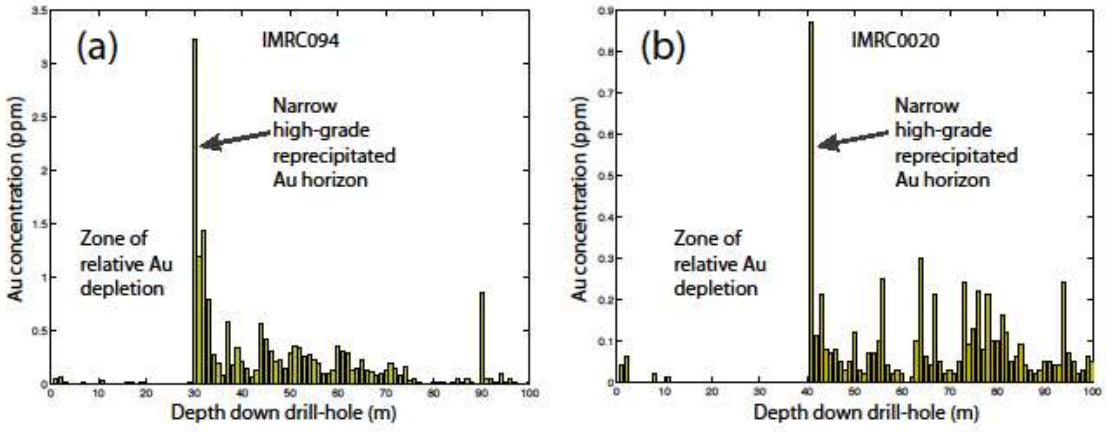

Figure 10.28. Down-hole drill core Au assay signals for holes IMRC094 (a) and IMRC0020 (b) from the Majestic prospect, Yindarlgooda dome. These are representative signatures of the relative Au depletion zone in the overlying lower saprolite zone and re-precipitation along the narrow high-grade zone around the water table. Note that the high-grade secondary enrichment zone produces higher grades than those within the hypogene section of the ore body below it. The zone of relative depletion in the lower saprolite produces some of the lowest grades within the drill-core interval, commonly lower than 0.1ppm.

10.10.3. Wavelet analysis of the supergene and regolith profiles at Majestic.

Figure 10.29 presents the results of wavelet-based analysis conducted upon the top 100m of 169 drill cores from Majestic (which incorporate the regolith profile, Au-Cu depleted lower saprolite and underlying supergene enrichment horizon) versus the 155 fresh rock results for the hypogene section of the system presented in previous sections. The upper 100m supergene part of the system is characterized by a much greater range in spectrum widths than the hypogene section, with a much

greater proportion of drill core intervals described by spectra with ranges greater than 3. The distribution of spectrum width in the supergene section of Majestic peaks in the range 2.5-3 with a mean of 3.7; whereas the hypogene section peaks in the range 1.5-2, with a mean of 2.54. The supergene section also possesses much greater variations in both left and right hand limb width than the hypogene section (Figure 10.29), with the supergene section being characterized by much greater widths in both limbs. The difference in width is most pronounced in the right hand limb, further reflected in the distribution of the spectrum asymmetry measure by a greater proportion of the supergene section showing stronger left handed asymmetry.

Both the supergene and hypogene sections of Majestic show almost identical distributions of α, f(α), and mean position, of the information dimension, D1 (Figure 10.29). D2 f(α) distributions between the two sections are almost identical. Both sections have D2(α) values that peak between 0-0.5; however, the supergene section has much greater proportions of spectra with values > 0.5. D0(α) values in the hypogene section peak in the range 1-1.5; whereas D0(α) values in the supergene section peak in the range 1.5-2, with a greater proportion with values > 2.

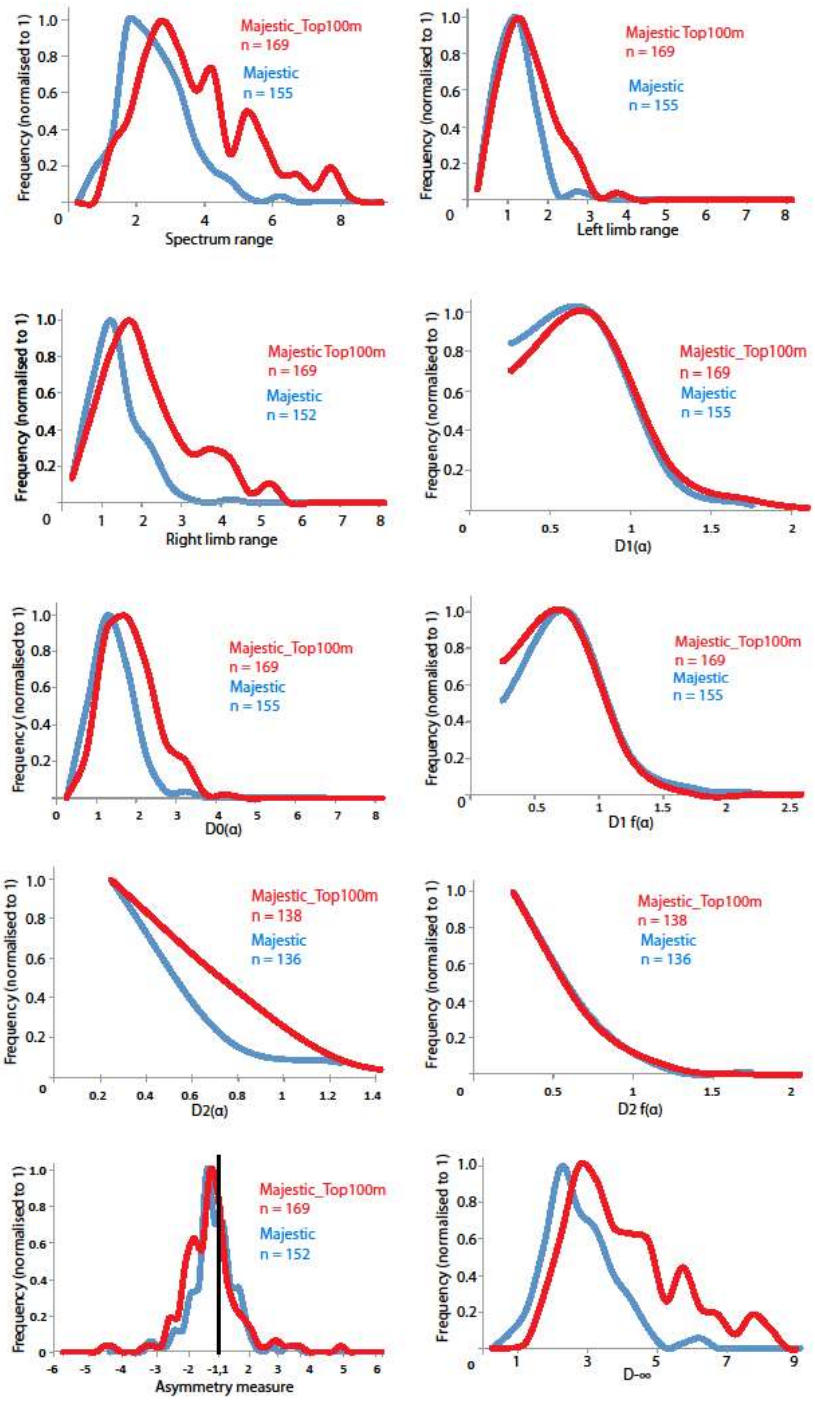

Figure 10.29. – Frequency normalized histograms comparing the distributions of singularity spectra metrics between the top 100m of drill cores from Majestic (incorporating the regolith and supergene sections of the system) and primary hypogene section of the system below the supergene enrichment horizon. Note that both sections of Majestic display similar behaviour with respect to D1(α), D1 f(α) and D2 f(α). The regolith and supergene sections of Majestic are characterised by a greater proportion of broader singularity spectra, and broader left and right hand limbs. The regolith and supergene sections also typically have higher D0(α) and D2(α) values. The supergene section has a greater proportion of left-handed asymmetry.

10.11. Implications for wavelet-based analysis of hydrothermal mineral systems.

Uplift, erosion and exposure of the Majestic system to surficial processes of the Yilgarn craton has lead to the eradication of primary hypogene textures in the upper part of the system via the leaching, and subsequent re-precipitation, of Au-Cu. This has modified the original Au assay signatures of the supergene section, and, therefore, the multifractal signatures that quantify it. Drill core intervals incorporating the regolith and supergene sections of the Majestic prospect are distinct from the lower primary hypogene section, showing greater singularity spectrum widths, left hand limb widths, right hand limb widths, greater asymmetry (left handed), and higher mean D0(α) and D2(α) values. The hypogene section of Majestic has a mean singularity spectrum width of 2.54, one of the multiple spectrum metrics that distinguish it from the Sunrise Dam ore bodies. However, the supergene section has a mean singularity spectrum width of 3.7, equivalent to ore bodies at Sunrise Dam.

Supergene processes have altered the Au assay signal in Majestic by two mechanisms: 1) the dissolution and elimination of Au in the lower saprolite, and 2) preferential re-precipitation of Au along a narrow horizon in concentrations higher than the primary ore body. Figure 10.30 represents this as a three-step process upon a synthetic Au signal to demonstrate how each of the two components above influences both the Au assay signal and multifractal signature of the upper section of a deposit. During both stages the signal below the supergene zone at 40m depth remains unaltered. The initial model possesses a relatively continuous signal and is composed of Au grades commonly detected within the Majestic prospect, and is quantified by a singularity spectrum that has a range of 1.92 – comparable to the Majestic hypogene system mean of 2.54. The system is subjected to oxidation processes and Au dissolution within the top 40m of the profile (applicable to the lower saprolite zone at Majestic), depleting Au to grades lower than those in the hypogene zone. This expands the range of the resultant singularity spectrum from 1.92 to 3.34. Au depletion enhances the multifractal signature of the system via the generation of additional sub-correlations within the assay signal at the new low-grades and the addition of discontinuities, rendering the signal more intermittent with a stronger hierarchical organisation.

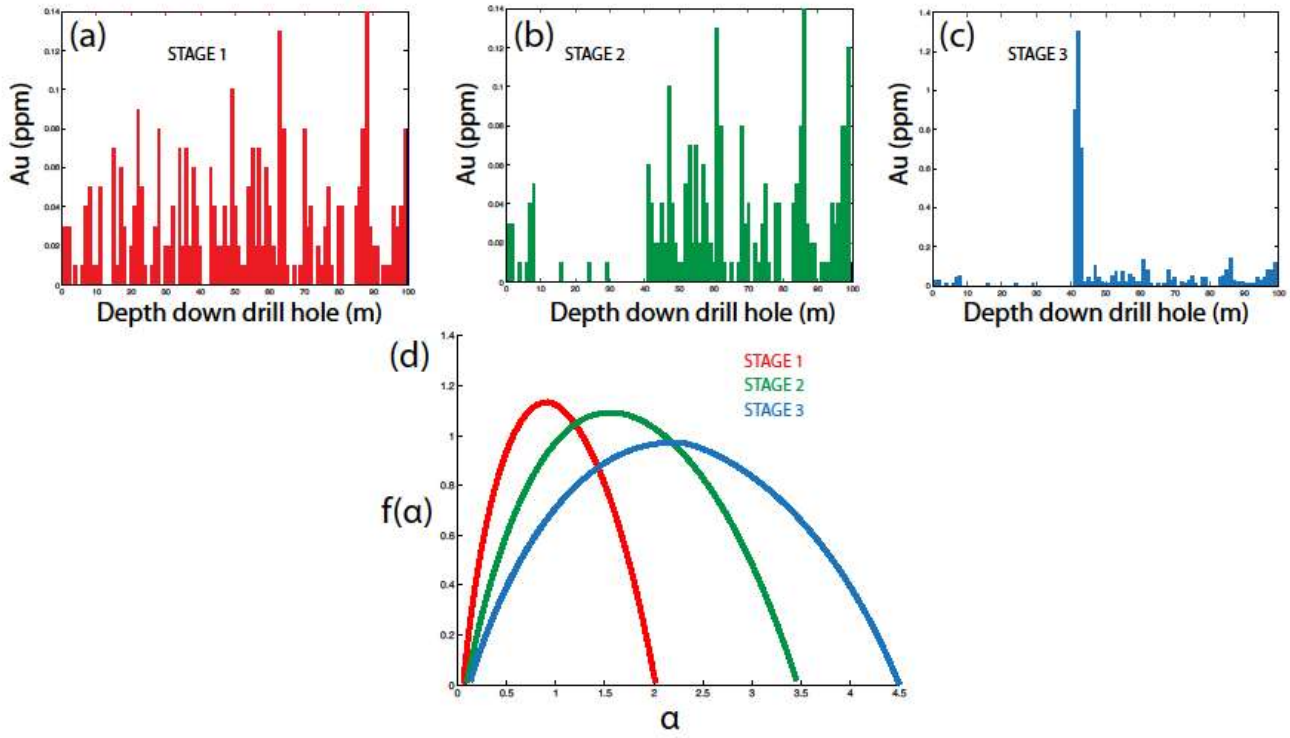

Figure 10.30. – (a) Stage 1 - a synthetic 100m Au assay representing primary mineralization within an ore body. It is characterized by a singularity spectrum with a range of 1.92 (d). (b) Stage 2 – Relative depletion of Au in the upper section of the deposit, following exposure to near surface conditions and interaction with meteoric fluids. This results in a very low-grade section of the interval relative to Au concentrations in the unaffected hypogene section of the deposit below it. Stage 2 oxidation processes and the remobilization of Au results in an expansion in the breadth of the singularity spectrum that describes the interval to 3.34 (d). (c) Stage 3 – preferential re-precipitation of remobilized Au along a narrow 3m-wide horizontal enrichment horizon at a depth of 40m. This results in a further expansion of the singularity spectrum to a range of 4.39. During stages 2 and 3 the signal below the depletion and enrichment profiles remains unmodified.

A subsequent stage of re-precipitation is then applied that generates a localised 3m-wide high-grade horizon at the base of the depleted zone, depositing grades at greater concentration than in the primary ore zone. The resultant singularity spectrum consequently expands in range again from 3.34 to 4.39. This increase occurs because the addition of a strong peak further increases the hierarchical structure of the drill-hole signal, in a similar manner to the tests of the effects of rare high-grade intersections in previous sections.

Broader singularity spectra in the supergene section of Majestic indicate that Au in this part of the system has a stronger hierarchical structure and is more irregular and intermittent than in the primary hypogene section. Spectra comparisons show that both the left and right hand limb components in the supergene section are broader. The left-hand limb of the singularity spectrum quantifies the low Au grades in the system; the left-hand limb quantifies the rare high Au grades. This signifies that spatial dynamics in both low and high Au grades in the supergene are more complex and correlate over greater ranges of wavelengths and amplitudes than their counterparts in the hypogene section. The difference in behaviour between the two sections is most pronounced in the broader right limb widths of the supergene section (i.e. dynamics of the high Au grades), consistent with it having a greater proportion of left-handed asymmetry. High Au grades in the supergene section of Majestic are therefore more irregular and intermittent than the low Au grades.

Larger left hand limbs in the supergene zone are driven by the relative depletion zone, which increases complexity in the low grades. Larger right hand limbs in the supergene zone are driven by re-precipitation along the 1-10km thick horizon, which increases complexity in the high grades. A greater relative increase in right limb width relative to the left suggests that concentrated re-precipitation has exerted a stronger impact upon the spectra than the initial depletion.

In reality the depletion and re-precipitation of Au in the supergene enrichment zone occur contemporaneously, however their isolation demonstrates the independent impact of each upon the signal. This investigation of the supergene processes at Majestic, and its influence upon the multifractal signature of an ore body has important implications for the use of wavelet-based analysis in characterizing the distributions of chemical species, ore minerals and the associated alteration assemblages within, and proximate to, ore bodies. Those conducting wavelet-based analysis should be mindful of the influence of secondary processes that overprint the primary signature of an ore body, and the position of the drill-core being analysed. Relative depletion and secondary enrichment under near surface conditions in the regolith profile may result in the ore body being characterized by a broader singularity spectrum than that of the primary hypogene system below it. They may also be described by significantly different singularity spectrum metrics (here D0, D2, left hand and right hand limb widths, and spectrum asymmetry). Although conducted upon Au assays in this investigation, these remobilization processes are also relevant to the spatial distribution of genetically related hydrothermal alteration phases such as sericite, chlorite, calcite and dolomite/ankerite. This is particularly important in Au assay, or hyperspectral mineral concentrations, derived from drill-holes that incorporate elements of both the core of an ore deposit and the surrounding 'regional' signature of a terrane. A sericite abundance signal at the margin of a hydrothermal deposit may be characterized by a more strongly developed hierarchical organization, with the 'regional' signature composed of relatively low-abundances and a locus of sericitization within the localised alteration zone having substantially higher abundances. This hybrid signature may therefore have a stronger multifractal signature than those that characterise either the 'region' or alteration zones independently.

10.12. Summary.

Ore bodies in the Yilgarn Craton of Western Australia are strongly multifractal, characterized by strong hierarchical spatial organisation. Comparison of the non-linear dynamics of seven deposits, determined by wavelet analysis, distinguishes three groups. Those examined from Sunrise Dam are more strongly multifractal (i.e. are characterized by broader ranges in $D_{-\infty}$ - $D_{+\infty}$) than those from the Yindarlgooda Dome (Salt Creek, Imperial and Majestic). Au in these ore bodies is therefore more irregularly distributed and correlates over a greater range of wavelengths and amplitudes. Additionally, the Cosmo East breccia lode at Sunrise Dam is more strongly multifractal and has more heterogeneous spatial dynamics than the other ore bodies from Sunrise Dam. Ore deposits with stronger multifractal signatures correspond to those with higher Au endowments and higher grades; those with narrower multifractal signatures are less endowed. Ore deposits exposed to strong lateritic weathering and meteoric fluids in near surface conditions in the Yilgarn craton may be subject to texturally destructive supergene processes. The selective dissolution, remobilization and re-precipitation of Au in these environments modify the multifractal signature of the deposit. A comparison of Au spatial dynamics in the secondary supergene zones of the Majestic system versus the primary hypogene zone shows that the supergene zone of a deposit may have a

significantly broader singularity spectrum signature than the primary deposit. This has implications for the use of wavelet analysis as an exploration tool in hydrothermal systems.

Recommended reading.

Afzal, P., Alghalandis, Y. F., Khakzad, A., Moarefvand, P., & Omran, N. R., 2011. Delineation of mineralization zones in porphyry Cu deposits by fractal concentration-volume modeling. Journal of Geochemical Exploration, **108**, 220–232.

Agterberg, F. P., 1995. Multifractal modeling of the sizes and grades of giant and supergiant deposits. International Geology Review, **37**, 1–8.

Arneodo, A., Audit, B., Decoster, N., Muzy, J-F. & Vaillant, C., 2002. Wavelet Based Multifractal Formalism: Applications to DNA Sequences, Satellite Images of the Cloud Structure, and Stock Market Data. In: Bunde, A., Kropp, J. & Schellnhuber, H. J., 2002. The Science of Disasters - Climate Disruptions, Heart Attacks, and Market Crashes. Springer Verlag, Berlin, 476pp.

Arneodo, A., Bacry, E. & Muzy, J. F., 1995. The thermodynamics of fractals revisited with wavelets. Physica A: Statistical Mechanics and its Applications, 213, 232-275.

Arneodo, A., Decoster, N., Kestener, P. & Roux, S. G., 2003. A Wavelet-Based Method for Multifractal Image Analysis: From Theoretical Concepts to Experimental Applications. Advances in imaging and electron physicstte, **126**, 1-92.

Arneodo, A., Vaillant, C., Audit, B., Argoul, F., d'Aubenton-Carafa, Y. & Thermes, C., 2011. Multi-scale coding of genomic information: From DNA sequence to genome structure and function. Physics reports, **498**, 45-188.

Bacry, E., 2009. LastWave 3.0 Reference Manual. http://www.cmap.polytechnique.fr/~bacry/LastWave/index.html

Baker, T., Bertelli, M., Blenkinsop, T., Cleverley, J., McLellan, J., Nugus, M. & Gillen, D., 2010. P-T-X Conditions of Fluids in the Sunrise Dam Gold Deposit, Western Australia, and Implications for the Interplay between Deformation and Fluids. Economic Geology, **105**, 873-894.

Beeson, J., 2010. Geological review of mineralization from selected drill holes, Majestic Prospect, Western Australia. Integra Mining Ltd internal geological report.

Behnia, S., Akhshani, A., Panahi, M., Mobaraki, A. & Ghaderian, M., 2012. Multifractal properties of denaturation process based on Peyrard–Bishop model. Physics Letters A, **376**, 2538-2547.

Blenkinsop, T.G., 1994. The fractal dimension of gold deposits: two examples from the Zimbabwe Archaean craton. In: Kruhl, J.H. (Ed.), Fractal and Dynamic Systems in Geosciences. Springer, Berlin, pp. 247–258.

Blenkinsop, T., Baker, T., McLellan, J., Cleverley, J. & Nugus, M., 2007. Sunrise Dam Gold Mine Geological Study Project. Project G15, pmdCRC.

Bolzan, M. J. A., Tardelli, A., Pillat, V. G., Fagundes P. R. & Rosa, R. R., 2013. Multifractal analysis of vertical total electron content (VTEC) at equatorial region and low latitude, during low solar activity. Annales Geophysicae, **31**, 127-133.

Brown, S. M., Fletcher, I. R., Stein, H. J., Snee, L. W., & Groves, D. I., 2002. Geochronological constraints on pre-, syn-, and postmineralization events at the world-class Cleo gold deposit, Eastern Goldfields province, Western Australia. Economic Geology, **97**, 541−559.

Carranza, E. J. M., 2009. Controls on mineral deposit occurrence inferred from analysis of their spatial pattern and spatial association with geological features. Ore Geology Reviews, **35**, 383–400.

Cheng, Q. M., 2007. Mapping singularities with stream sediment geochemical data for prediction of undiscovered mineral deposits in Gejiu, Yunnan Province, China. Ore Geology Reviews, **32**, 314–324.

Cheng, Q. M., Agterberg, F. P., 2009. Singularity analysis of ore-mineral and toxic trace elements in stream sediments. Computers & Geosciences, **35**, 234–244.

Cloke, P. L. & Kelly, W. C., 1964. Solubility of gold under inorganic supergene conditions. Economic Geology, **59**, 259-270.

Czarnecki, L. & Grech, D., 2010. Multifractal Dynamics of Stock Markets. Acta Physica Polonica A, **117**, 623-629.

Ford, A. & Blenkinsop, T. G., 2008. Combining fractal analysis of mineral deposit clustering with weights of evidence to evaluate patterns of mineralization: application to copper deposits of the Mount Isa Inlier, NW Queensland, Australia. Ore Geology Reviews, **33**, 435–450.

Gaillot, P., Darrozes, J & Bouchez, J-L., 1999. Wavelet transform: a future of rock fabric analysis? Journal of Structural Geology, **21**, 1615-1621.

Hill, E. J., Oliver, N. H. S., Cleverley, J. S., Nugus, M. J., Carswell, J. & Clark, F., 2014. Characterisation and 3D modelling of a nuggety, vein-hosted gold ore body, Sunrise Dam, Western Australia. Journal of Structural Geology, **67**, 222-234.

Hodkiewicz, P. F., Weinberg, R. F., Gardoll, S. J. & Groves, D. I., 2005. Complexity gradients in the Yilgarn craton: fundamental controls on crustal scale fluid-flow and the formation of world-class orogenic-gold deposits. Australian Journal of Earth Sciences, **52**, 831-841.

Ivanov, P. Ch., Amaral, L. A. N., Goldberger, A. L., Havlin, S., Rosenblum, M. G., Struzik, Z. R., & Stanley, H. E., 1999. Multifractality in human heartbeat dynamics. Letters to Nature, **399**, 461-465.

Lewis, M. J. & McNarry, M. A., 2013. Influence of age and aerobic fitness on the multifractal characteristics of electrocardiographic RR time-series. Frontiers in Physiology, 4, Article 100.

Mann, A. W., 1984. Mobility of gold and silver in lateritic weathering profiles: some observations from Western Australia. Economic Geology, **79**, 38-49.

Meneveau, C. & Sreenivasan, K. R., 1991. The multifractal nature of turbulent energy dissipation. Journal of Fluid Mechanics, **224**, 429-484.

Miller, J. McL. & Nugus, M., 2006. The structural evolution of the Sunrise Shear Zone and the overlying Watu and Western Shear Zones, Sunrise Dam gold Deposit, Laverton, W.A. Project Y4, pmdCRC.

Monecke, T., Gemmell, J. B. & Monecke, J., 2001. Fractal distributions of veins in drill core from the Hellyer VHMS deposit, Australia: constraints on the origin and evolution of the mineralising system. Mineralium Deposita, 36, 406-415.

Mueller, A. G., 2011. Chronologic sequence of diorite intrusion, wall-rock alteration and Cu-Au mineralization in the Majestic porphyry complex, Mt Monger, Eastern Goldfields, Western Australia. Integra Mining Ltd internal geological report.

Ord A., Munro M., & Hobbs, B. E., in press. Hydrothermal mineralising systems as chemical reactors. Ore Geology Reviews, in press.

Ouillon, G. & Sornette, D., 1996. Unbiased multifractal analysis: Application to fault patterns. Geophysical Research Letters, 23, 3409-3412.

Pavlov, A. N. & Anishchenko, V. S., 2007. Multifractal analysis of complex signals. Physics-Uspekhi, 50, 819-834.

Ramirez-Rojas, A., Munoz-Diosdado, A., Pavia-Miller, C. G. & Angulo-Brown, F., 2004. Spectral and multifractal study of electroseismic time series associated to the M_w=6.5 earthquake of 24 October 1993 in Mexico. Natural Hazards and Earth System Sciences, 4, 703-709.

Rinaldo, A., Rodriguez-Iturbe, I., Rigon, R., Bras, R. L., Ijjasz-Vasquez, E. & Marani, A., 1992. Minimum Energy and Fractal Structures of Drainage Networks. Water Resources Research, **28**, 2183-2195.

Robb, L., 2005. Introduction to ore-forming processes. Blackwell publishing, 373pp**.**

Stanley, H. E., Amaral, L. A. N., Goldberger, A. L., Havlin, S., Ivanov, P. Ch. & Peng, C.-K., 1999. Statistical physics and physiology: Monofractal and multifractal approaches. Physica A, **270**, 309-324.

Sun, T. & Liu, L., 2014. Delineating the complexity of Cu–Mo mineralization in a porphyry intrusion by computational and fractal modeling: A case study of the Chehugou deposit in the Chifeng district, Inner Mongolia, China. Journal of Geochemical Exploration, **144**, 128-143.

Turiel, A., Perez-Vincente, C. J. & Grazzini, J., 2006. Numerical methods for the estimation of multifractal singularity spectra on sampled data: A comparative study. Journal of Computational Physics, 216, 362-390.

Wang, G. & Ren, D., 2013. Classification of surface electromyographic signals by means of multifractal singularity spectrum. Medical & Biological Engineering & Computing, 51, 277-284.

Wang, G., Carranza, E. J. M., Zuo, R. G., Hao, Y. L., Du, Y. S., Pang, Z. S., Sun, Y. & Qu, J. N., 2012. Mapping of district-scale potential targets using fractal models. Journal of Geochemical Exploration, **122**, 34–46.

Wang, Q., Deng, J., Liu, H., Yang, L., Wan, L. & Zhang, R., 2010. Fractal models for ore reserve estimation. Ore Geology Reviews, **37**, 2-14.

Williams, A., 2014. A microstructural and geochemical study of the Sunrise Dam Gold Deposit, Western Australia: Insights gained into the hydrothermal alteration of fluids in relation to gold mineralization. Unpublished Masters thesis, Macquarie University, Sydney.

Young, C., 2012. The Archaean Majestic Au-Cu Deposit, Eastern Goldfields, Western Australia, Characteristics and

implications for genesis. Red Metals Symposium presentation.

Zuo, R., Cheng, Q. & Xia, Q., 2009. Application of fractal models to characterization of vertical distribution of geochemical element concentration. Journal of Geochemical Exploration, **102**, 37-43.